Centrifuge Testing of an Expansive Clay

by

Michael David Plaisted, B.S.

Thesis

Presented to the Faculty of the Graduate School of

The University of Texas at Austin

in Partial Fulfillment

of the Requirements

for the Degree of

Master of Science in Engineering

The University of Texas at Austin

August 2009

Centrifuge Testing of an Expansive Clay

Approved by
Supervising Committee:

Jorge G. Zornberg

Robert B. Gilbert

Acknowledgments

I would like to thank my family and friends for their support throughout graduate school. Thanks also goes to Dr. Jorge Zornberg for his guidance, Jeff Kuhn for his help with research and soil characterization, Carlos Guzman for help with free swell testing, Albert Kottke and Mark Kroncke for help with LaTeX, the research group for feedback during seminars, and the Texas Department of Transportation for funding of my research.

MICHAEL DAVID PLAISTED

The University of Texas at Austin

August 2009

Centrifuge Testing of an Expansive Clay

Michael David Plaisted, M.S.E.
The University of Texas at Austin, 2009

Supervisor: Jorge G. Zornberg

Expansive clays are located world wide and cause billions of dollars in damage each year. Currently, the expansion is usually estimated using correlations instead of direct testing as direct testing is expensive and often takes over a month to complete. The purpose of this study was to determine if centrifuge technology could be used to characterize expansive clays through direct testing.

Testing was performed in an centrifuge permeameter on compacted specimens of Eagle Ford clay. A framework was developed to analyze effective stresses in centrifuge samples and methods were proposed to determine the swell-stress curve of a soil from centrifuge tests. Standard free swell test were also performed for comparison.

The swell-stress curve determined by centrifuge testing was found to match with the curve found from free swell tests after correcting for differences in testing procedures. The centrifuge tests were found to be repeatable and required several days for testing rather than weeks.

Contents

List of Tables

List of Figures

Chapter 1

Introduction

1.1 Motivation

Expansive soils are common throughout the United States and cause extensive damage to structures built on them. Jones and Holtz [1973] estimated yearly losses in the United States of over $2 billion (1970 dollars). Further studies (Olson [2009]) suggest that Jones and Holtz significantly underestimated these losses. Regardless of the exact number, damage from expansive clays is one of the most significant sources of damage for roadways and foundations in the United States.

The need to characterize the swelling potential of clays in design is obvious. If the maximum volume change is known the structure can be designed to withstand this movement. The Texas Department of Transportation (TxDOT) has found roadways built on expansive clays problematic and has funded research projects to mitigate damage of pavements from subgrade movement. TxDOT also developed the Potential Vertical Rise (PVR) method to determine the total swelling potential of a subgrade. Recently, TxDOT began implementing a modified PVR method that characterizes the swelling potential of clay by relating the swell to measured soil

suction values. It is the opinion of the author that swelling properties should be measured directly rather than through indirect correlations.

Direct testing of swell potential in expansive clays has generally focused on the use of consolidation frames to measure the volume change of soil when water is absorbed. These tests often take weeks or months to complete resulting in high costs. Due to the significant time demands, indirect methods such as the PVR are often used instead. There is a need for a method to directly measure the swelling potential of expansive soils while remaining expeditious so that the method is not neglected and correlations used instead.

There has been limited use of centrifuge technology with swelling clays and this research project intends to explore the use of this technology. The University of Texas at Austin has acquired a small inexpensive centrifuge and the use of the centrifuge for the testing of expansive clays will be evaluated. It is hoped that centrifuge technology can be shown to reliably measure the swelling potential of expansive clays. In addition, the test should be cost effective compared to alternatives. If this is accomplished and direct measurement of swelling is adopted rather than its prediction based on index properties, the accuracy of swell prediction in field cases should be significantly increased.

1.2 Scope of Research

The research study involved the testing of expansive clay in an increased gravitational field due to centrifugation. Tests were performed by ponding water on top of compacted specimens and spinning them in a centrifuge until an equilibrium swell was achieved. The expansive clay was also tested using standard free swell procedures and ultimate swelling from both procedures were compared. No attempt

was made to compare the swell of samples over time. The focus of the study was on the final swell of samples and using the measured swells to predict the entire swell-stress relation of soils.

1.3 Organization of Thesis

This thesis has been divided into six chapters. This first chapter includes the introduction material such as motivation and scope. Chapter 2 is a review of literature pertaining to expansive clays and centrifuge testing. Chapter 3 includes a soil characterization of the Eagle Ford clay used in the testing program. The soil characterization includes an expansive characterization of the soil using standard free swell tests. The centrifuge equipment is discussed in detail in Chapter 4. The testing procedure used in the main testing program of this research is also discussed in Chapter 4. The testing program and results are included as Chapter 5.

Chapter 6 is the main section of the thesis where the testing program results are analyzed. The accuracy of measurements, consistency of compaction and results are discussed. A framework to analyze stresses in centrifuge samples is suggested and a method for determining the swell-stress relation of soils using centrifuge test results is discussed. Finally a comparison of centrifuge test results and free swell tests was performed.

The conclusions of the research and suggestions for future study completes the thesis as Chapter 7.

Chapter 2

Background Information

2.1 Expansive Clays

2.1.1 Location

While the Eagle Ford clay used in this study was obtained from central Texas, expansive clays are not unique to Texas. A study by Krohn and Slosson [1980] found expansive clays to be distributed throughout the entire United States. Several areas with an abundance of expansive clay are found in Texas, California, North Dakota, and Kansas. An illustration from Krohn and Slossen of the location of expansive clays is included as Fig. 2.1.

Expansive clays are also found world wide, as indicated by course notes from Olson on Foundation Design Associated with Expansive Clay (Olson [2009]). Specifically problems with expansive clays have been reported from countries including Africa, Australia, Israel, India, and China. Searches for articles on expansive clay damage (using Engineering Village) results in thousands of hits with case studies from around the world.

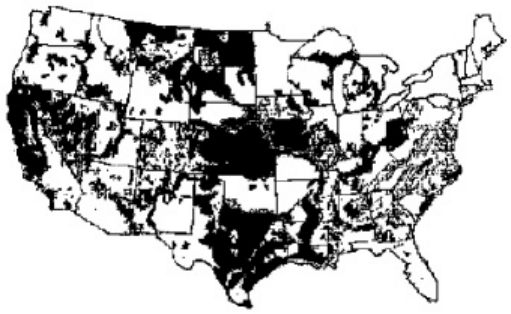

Figure 2.1: Expansive clays in the United States (Krohn and Slosson [1980])

2.1.2 Moisture Variation

In order for expansive soils to be of problem they generally must be located in an area with seasonal wetting and drying. In the United States, Texas and California are two major areas that have both an abundance of expansive clays and the climate to promote damage from them. Of interest in areas with seasonal wetting and drying is the depth of the *active zone*. The active zone is the section of a soil profile which undergoes significant seasonal variations in water content (Olson [2009]) and is where soil expansion mainly occurs. The depth of the active zone varies depending on climate and is generally on the order of 10 feet. However O'Neill and Poormoayd (1980) reported depths as large at 30 feet in San Antonio, Texas. Other causes for moisture variation in soils beyond what is expected due to seasonal changes include irrigation, run off from houses, vegetation absorbing water, wells, and many others.

2.1.3 Swell Relationships

Much research has been done in an attempt to relate the swell of an expansive clay to standard index properties. McDowell (1956) provided relations of potential

Table 2.1: Common Swell Relations

Source	Properties	Correlation
Vijayvergiya & Ghazzalay (1973)	Liquid limit, w_L (%) Dry unit weight, γ_d (lb/ft^3)	$log\, S\% = \frac{1}{19.5}(\gamma_d + 0.65 w_L - 130.5)$
Nayak & Christensen (1974)	Plasticity index, I_p (%) Initial water content, w_i (%) Clay content, C	$S\% = 2.3 * 10^{-2}(I_p)^{1.45}(\frac{C}{w_i}) + 6.4$
McDowell (1956)	Plasticity index, PI (%)	$S\% = 0.22PI - 2.8$ (at optimum W_c)
Rao et al. (2004)	Dry unit weight, γ_{di} (kN/m^3) Initial water content, w_i (%) Overburden pressure, q_i (kPa) Free swell index, FSI	$S\% = 4.24\gamma_{di} - 0.47 w_i - 0.14 q_i + 0.06(FSI) - 55$

swell based on plasticity index and wetness of soil. Vijayavergiya and Ghazzaly [1973] and Nayak and Christensen [1974] suggested relations using the dry unit weight and either the plasticity index or liquid limit. Rao et al. [2004] showed that basing the relation on dry unit weight, compaction water content, overburden pressure, and free swell index resulted in higher accuracy than the previous relations. The free swell index used in Rao et al. [2004] calculation is calculated as:

$$FSI = \frac{(V_w - V_k) \times 100}{V_k} \tag{2.1}$$

where V_w and V_k are the volume of a soil mass passing a 425 μm sieve in water and kerosene respectively. Table 2.1 includes the correlations for the swell predictions discussed.

2.1.4 Direct Testing

2.1.4.1 Free Swell Test

The free swell test (ASTM D 4546-08) is performed in a standard consolidation frame. The standard contains three methods for performing free swell test. Method A is the most common and can be referred to as *wetting-after-loading on multiple specimens.* The method requires at least four specimens to be compacted and tested at varied overburden pressures. The minimum sample height and diameter are 20mm and 50mm respectively. The overburden pressure are applied and the samples allowed to densify. When densification is completed water is added and swell measured at times of 0.5, 1, 2, 4, 8, 15 minutes and so on, up to generally between 24 and 72 hours or when the majority of swelling has occurred. The resulting swells can then be plotted against vertical stress as seen in Fig. 2.2. The swell pressure can be calculated by interpolating the overburden pressure that would result in zero swell.

Method B is similar to Method A however is performed on a single *in-situ* field sample and consolidated at an overburden pressure to match field stresses. Method C involves wetting the sample and measuring swell and then adding the desired overburden pressure. This is done to match cases where structures are built on already expanded soils and is essentially a consolidation test.

2.1.4.2 Swell Pressure Testing

The swell pressure can be measured directly using a procedure similar to the free swell test method A. However instead of a constant overburden pressure, the pressure is continuously adjusted as to hold the sample height unchanged. The samples typically reach equilibrium within 24 hours (Olson [2009]) and the overburden

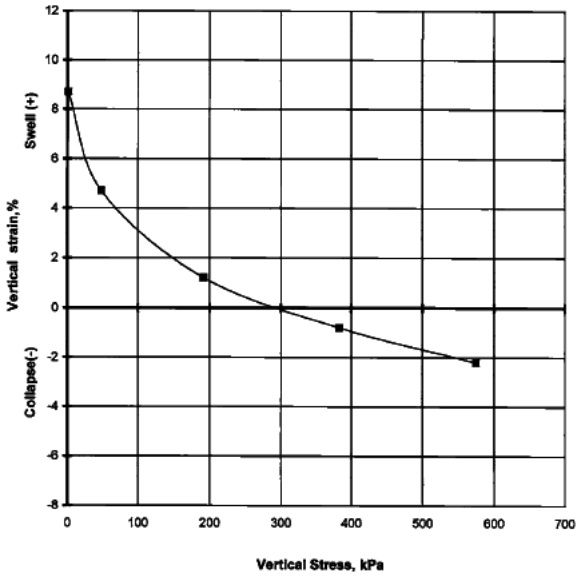

Figure 2.2: Plotted Free Swell Tests, Method A (ASTM D 4546-08)

pressure at equilibrium is the swell pressure. For the testing of solely swell pressure this method is often preferred over ASTM D 4546 Method A as only one sample is required to obtain the swell pressure.

2.1.5 Implementations

2.1.5.1 Potential Vertical Rise Method

The Potential Vertical Rise (PVR) method has been widely used by the Texas Department of Transportation for the estimation of surface movement due to expansive soils. The method is adapted from the research of C. McDowell and has several notable limitations:

- The predicted swell is based solely on the plasticity index. Recent research (see Section 2.1.3) has shown dependence on many other factors.

- The data set was populated using results from tests with soils locally to Guadalupe County, Texas. The applicability to other regions, even in Texas, is questionable. The relations have also been extrapolated far past where any data was collected (see Fig. 2.3a)

- The method assumes water is readily available for the entire soil profile. It does not consider an active zone.

Despite the limitations the method has been extensively used in Texas and is worth review. The PVR method divides the soil profile into two feet sections. For each section a water content, liquid limit, plasticity index, unit weight, and percent finer than #40 sieve should be known. The soil in each layer is then classified as "wet", "average", or "dry" based on a comparison of the measured water content with relations based on the liquid limit for the layer. If the measured water content is around or below the value calculated using Equation 2.2 the soil is considered "dry". Measured water contents between Equations 2.2 and 2.3 are considered "average" and measured water contents around and above values calculated with Equation 2.3 are considered "wet".

$$\omega_{dry} = 0.2LL + 9 \tag{2.2}$$

$$\omega_{wet} = 0.45LL + 2 \tag{2.3}$$

Figure 2.3a is then used to calculate the percent volume change of each layer based on its soil moisture classification (dry, average, or wet) and the plasticity index. The percent volume changes are however for a soil with an overburden pressure of 1 psi and must be corrected to a "free swell" using Equation 2.4.

$$Freeswell = (S\%\, at\, 1psi)(1.07) + 2.6 \tag{2.4}$$

Once the calculated "free swell" for each layer has been determined, Fig. 2.3b is used to calculate the PVR at the top and base of each layer. The stresses used to determine the PVR in Fig. 2.3b should be the calculated effective stresses at the top and the base assuming a unit weight of 125 pcf. The difference of the PVR at the base and top of layer is then considered the swell for that layer. The swell for each layer is then corrected for the actual unit weight (as 125pcf was assumed in calculations) and the percent finer than a #40 sieve.

2.1.5.2 O'Neill and Poormoayed

In an article by O'Neill and Poormoayed [1980] a method for calculating total surface swell was introduced. The method was based on research for foundation design and had improvements over the PVR method in that it includes the depth of the active zone. The method also uses the water content directly rather than classifying it as wet, average, or dry. According the their method, the total swell at the surface in inches can be calculated by:

$$S = 0.0396 D_{AZ} 10^{0.4787 + 0.0329 LL - 0.0821 W_c} \tag{2.5}$$

where D_{AZ} is the depth of the active zone in feet, and LL and W_c are the liquid limit and natural water content of the soil as a percentage. Graphs of relations obtained using Equation 2.5 did not include actual data so the scatter and range of data used in unknown. The method also requires an average liquid limit and water content of the active zone where the PVR method breaks the soil profile into discrete layers.

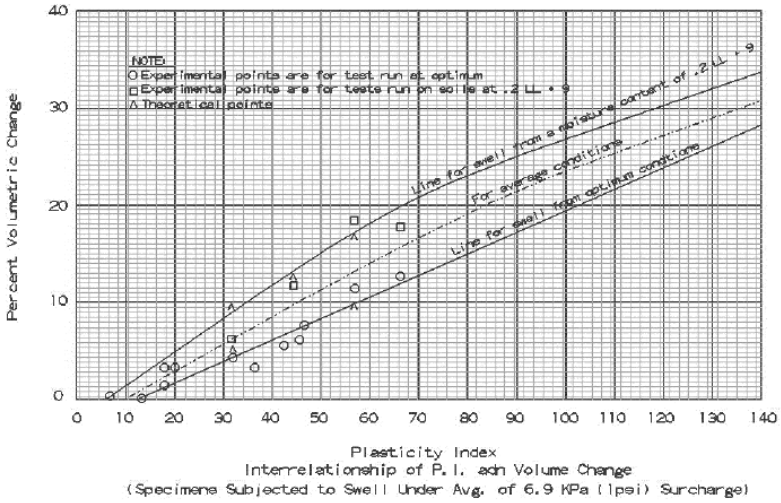

(a) Relation of P.I. and Volume Change

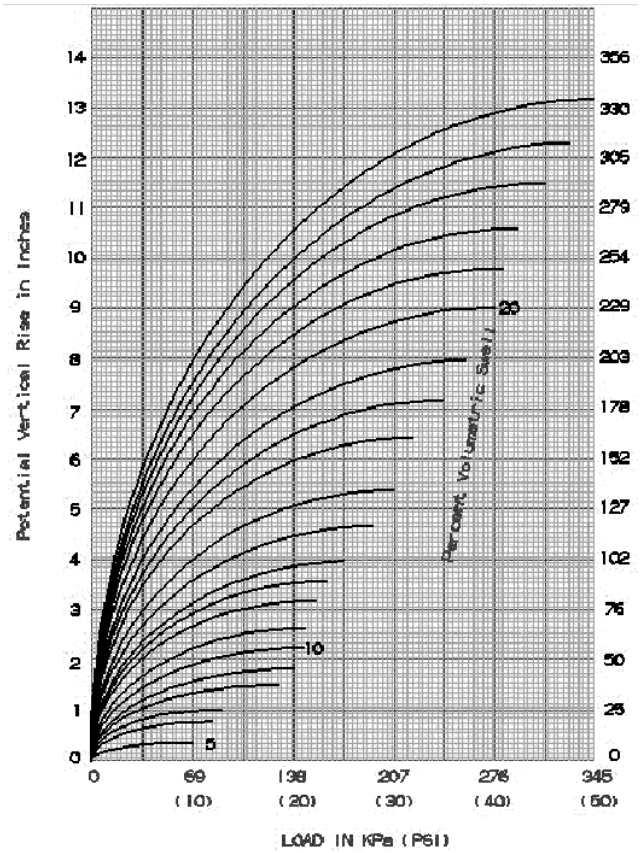

(b) Relation of Load to Potential Vertical Rise

Figure 2.3: Potential Vertical Rise (TEX-124-E)

2.1.5.3 Potential Vertical Rise Revisited

The PVR method discussed in Section 2.1.5.1 was revisited by Lytton et al. [2006]. They concluded that the current PVR method generally overestimated swell in the field and the assumptions made by the method were problematic. A new method was proposed to estimate surface swell. The method was based on a finite difference model of the soil profile. In the finite difference model moisture movement was calculated throughout the profile based on plausible weather and climate data resulting in suction profiles over time. The calculated suctions were then used to predict swell.

In order to model the movement of moisture in the soil the diffusion coefficient, α, is required. Lytton et al. [2006] proposed an evaporation test in which the suction of a soil sample at constant temperature is monitored over time by thermocouple psychrometers. The measured suctions are then plotted and the diffusion coefficient is chosen for a best fit.

The suctions that are calculated for the soil profile using the measured diffusion coefficient must then be related to volume changes. The model proposed is:

$$\frac{\triangle V}{V} = -\gamma_h log\frac{h_f}{h_i} - \gamma_\sigma log\frac{\sigma_f}{\sigma_i} - \gamma_\pi log\frac{\pi_f}{\pi_i} \tag{2.6}$$

where γ_h, γ_σ, and γ_π are the matric suction, mean principal stress, and the osmotic suction compression indexes. $h_{f,i}$, $\sigma_{f,i}$, $\pi_{f,i}$ are the final and initial matric suction, mean principal stress, and osmotic suction. Since the osmotic suction changes are negligible the term is removed. The calculated volume change is related to vertical strain as:

$$\frac{\triangle H}{H} = f\left(\frac{\triangle V}{V}\right) \tag{2.7}$$

where f is 0.5 for drying and 0.8 for wetting.

The compression indexes are needed for the calculation of volume change. In the method suggested by Lytton et al. [2006] both of the required indexes, γ_h and γ_σ, are calculated based on several correlation with the liquid limit, plasticity index, percent finer than #200 sieve, and percent finer than 2 microns. The soil must first be classified according to the Holtz and Kovacs mineral classification chart (Figure 2.4a). Charts specific to each mineral classification are used to relate the activity of the clay and the liquid limit to a soil compression index, γ_o. A chart for Zone II minerals is included for reference in Fig. 2.4b. The matric suction compression index, γ_h, is then calculated from γ_o using the correlation:

$$\gamma_h = \gamma_o \left[\frac{\% - 2micron}{\% - \#200}\right] \tag{2.8}$$

where %-2micron and %-#200 and the percent finer than a 2 micron and #200 sieve respectively. The mean principal stress compression index is then calculated from γ_h using:

$$\gamma_\sigma = \gamma_h \frac{1}{1 + \frac{h}{\theta\left(\frac{\delta h}{\delta \theta}\right)}} \tag{2.9}$$

$$\left(\frac{\delta h}{\delta \theta}\right) = \frac{1}{0.4343}\frac{S\gamma_w}{\gamma_d}h \tag{2.10}$$

$$S = -20.29 + 0.15555LL - 0.117PI + 0.0184\,(\% - \#200) \tag{2.11}$$

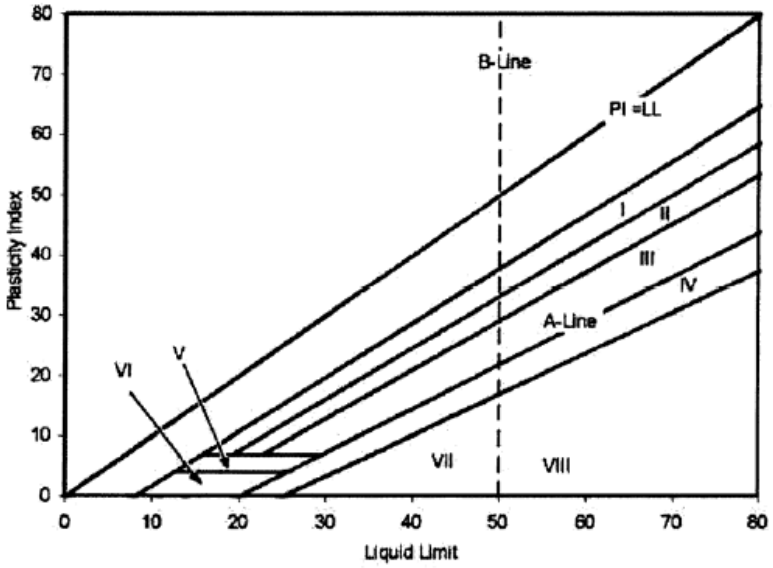

(a) Soil Characterization

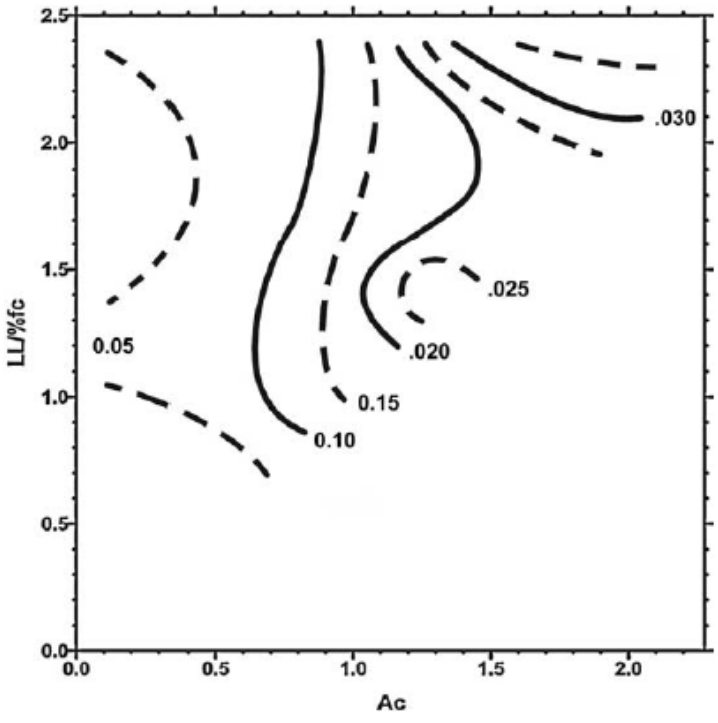

(b) Zone II Chart for Determining γ_o

Figure 2.4: PVR Revisited Graphs Lytton et al. [2006]

where h is the matric suction, γ_w is the unit weight of water, γ_d is the dry density of soil, and LL and PI are the liquid limit and plasticity index. Several other corrections based on soil properties can be applied.

The main issue with the revised PVR procedure is that the only parameter measured other than index properties is the suction over time of the soil in the evaporation test. This test is only used to calibrate the moisture movement model to predict suctions. The entire relation between suction and actual volume changes is based off of multiple empirical equations. It is not known how much scatter each empirical formula includes and when the prediction of one equation is used as input to another the possibility for very high scatter occurs. These problems could be avoided if the swell of the clay was measured directly.

2.2 Centrifuge Testing

Geotechnical centrifuge testing has generally been associated with mechanical aspects such as the scale model testing of retaining walls or slopes. However there has been interest in using the increased gravitation field of the centrifuge to accelerate flow processes. The use of centrifuging to accelerate flow has been widely used in the oil industry however Cargill and Ko (1983) and Nimmo et al. [1987] were of the first to use centrifuges for geotechnical flow purposes.

Nimmo et al. [1987] showed that steady state one dimensional unsaturated flow could be accomplished in the centrifuge. Samples were spun at g levels ranging from approximately 220 to 1650 and flow rates were consistent with Darcy's law. Theoretical and experimental suction profiles showed good correlation. Testing of samples with hydraulic conductivities on the order of $1 \times 10^{-11} m/s$ came to equilibrium within 24 hours. Recently, Singh and Kuriyan [2002] and further

studies by Nimmo (Caputo and Nimmo [2005], Simunek and Nimmo [2005]) have expanded on the use of centrifuging for unsaturated flow purposes.

Dell'Avanzi et al. [2004] developed a framework for analysis of unsaturated soils using gradient in fluid potential as the driving mechanism. Following Dell'Avanzi et al. [2004] framework the potential for a fluid is:

$$\phi_m = gz_m + \frac{1}{2}\left(\frac{v_m}{n}\right)^2 - \frac{\psi_m}{\rho_w} \tag{2.12}$$

where g is the acceleration due to gravity, z_m is the distance above the datum, v_m is the discharge velocity, n is the soil porosity, ψ_m is the total suction, and ρ_w is the density of water. In unsaturated soils the discharge velocity, v_m, is low enough that the second term can be ignored resulting in:

$$\phi_m = gz_m - \frac{\psi_m}{\rho_w} \tag{2.13}$$

The potential due to elevation in 1g, gz_m, must be modified to incorporate a linearly increasing g level. The g level in a centrifuge is dependent on the rotational velocity ω and the radius r such that the acceleration experienced at a radius r in the centrifuge is:

$$a_m = \omega^2 r \tag{2.14}$$

Therefore the elevation potential in the centrifuge can be calculated by integrating the g level across the radius such that elevation potential:

$$\phi_{e,m} = -\frac{1}{2}\omega^2(r_0 - z_m)^2 \tag{2.15}$$

where r_0 is the radius of the datum. Replacing the elevation potential term in Equa-

tion 2.13 with Equation 2.15 results in the total fluid potential of a sample in the centrifuge as:

$$\phi_m = -\frac{1}{2}\omega^2(r_0 - z_m)^2 - \frac{\psi_m}{\rho_w} \tag{2.16}$$

Flow in a unsaturated sample with a area A_m is governed by Darcy's law such that:

$$Q_m = -\frac{k(\psi)}{g}\frac{\delta\phi_m}{\delta z_m}A_m \tag{2.17}$$

Dividing Equation 2.17 by the area results in the seepage velocity:

$$v_m = -\frac{k(\psi)}{g}\frac{\delta\phi_m}{\delta z_m} \tag{2.18}$$

Taking the derivative of Equation 2.16 with respect to centrifuge radius $z_m$and substituting into Equation 2.18 for $\frac{\delta\phi_m}{\delta z_m}$ results in the seepage velocity of a centrifuge sample:

$$v_m = -\frac{k(\psi)}{\rho_w g}\left(\rho_w\omega^2(r_0 - z_m) - \frac{\delta\psi_m}{\delta z_m}\right) \tag{2.19}$$

This framework was later used by McCartney [2007] in the development of a fully instrumented centrifuge permeameter that was capable of quickly characterizing the water retention curve and k-function of unsaturated soils.

2.2.1 Darcy's Law

Centrifuges have also been used for the measurement of saturated hydraulic conductivity. Nimmo and Mello [1991] and Singh and Gupta [2000] showed that flow rate in the centrifuge, v_m, scaled with the increase in gravity, N, such that

$$v_m = Nv \tag{2.20}$$

where v is the flow rate in a 1g test. In published notes on Singh and Gupta [2000], Sharma and Samarasekera [2007] inferred that since the hydraulic gradient is a dimensionless quantity (ratio of two lengths) it is the same for centrifuge and 1g tests. This lead to the conclusion, based on Darcy's Law, that the hydraulic conductivity in the centrifuge model is N times larger than the 1g model. This is in agreement with others (Cargill and Ko [1983], Tan and Scott [1985], Singh and Gupta [2000]) who also concluded that Darcy's permeability scales with g level. However other researchers (Goodings [1985], Taylor [1985], Dell'Avanzi et al. [2004]) have indicated that the gradient, rather than the hydraulic conductivity, should be scaled resulting in the hydraulic conductivity being independent of gravity.

Thusyanthan and Madabhushi [2003] reported that the source of this confusion stemmed from the conventional definitions of hydraulic gradient and Darcy's permeability where the driving force due to gravity is included in the permeability as the unit weight of the fluid. Following a derivation similar to Dell'Avanzi et al. [2004] except for saturated soils, Thusyanthan and Madabhushi [2003] concluded that flow in a centrifuge should be calculated using:

$$v = \frac{k_{1g}}{\gamma_{1g}} \times \frac{\triangle[P + z\rho g]}{\triangle L} \tag{2.21}$$

where k_{1g} and γ_{1g} are the saturated hydraulic conductivity and unit weight under 1g conditions. Using Eqn. 2.21 for saturated flow, Darcy's permeability becomes independent of g level and the increase in energy gradient is the clear cause for increased flow rates.

It is concluded that the scaling of gradient rather than hydraulic conductivity is the appropriate method for the use of Darcy's law in the centrifuge. The hydraulic conductivity should be a constant regardless of g level. Theoretically if a sample was tested in a zero g environment with an imposed pressure gradient, the notation used by Sharma and Samarasekera [2007] and others would calculate that the hydraulic conductivity is zero and no flow could occur. Obviously a porous soil could have a flow rate under solely a pressure gradient and this shows the fallacy in the scaling of permeability rather than gradient.

2.2.2 Swelling Clays

There has been little published testing of expansive clays in the centrifuge. Frydman and Weisberg [1991] were the first to explore the use of centrifuge technology for expansive soils. Testing was performed on Mizra clay, a highly plastic montmorillonite clay found in Israel. The soil contained approximately 70% clay particles, a liquid limit of 78%, and a plasticity index of 53%. Tests were run on 300 mm high columns of soil with water ponded on top with a free draining base. Steel balls were placed throughout the sample and scanned with gamma rays to get incremental strain readings and water contents.

The resulting swell-stress relation from the centrifuge tests (Fig. 2.5) correlated roughly with data obtained from 1g consolidometer tests. However at low stresses the centrifuge tests swelled more and at high stresses the centrifuge tests swelled less in comparison with the 1g relation. Frydman and Weisberg [1991] attributed the differences to side friction. The data for low stresses came from the upper portion of the column where there was little surface area for frictional interaction and the consolidometer tests likely experienced higher friction. The data

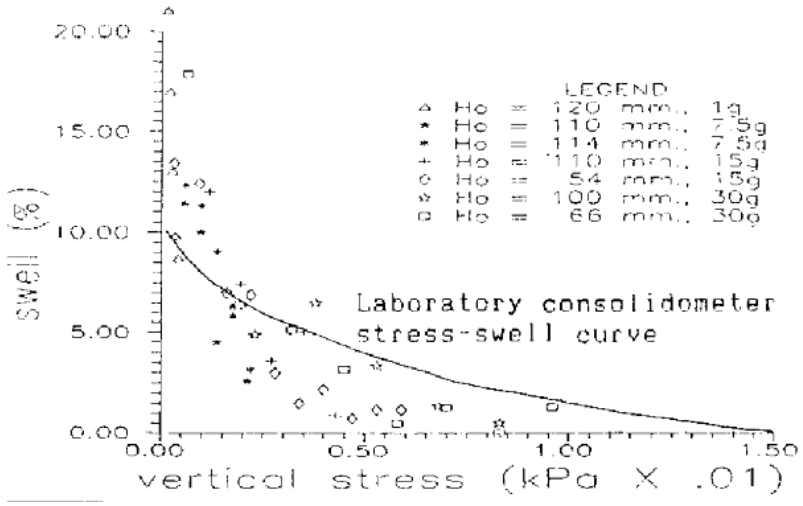

Figure 2.5: Swell-Stress Relation (Frydman and Weisberg [1991])

for higher stresses came from the lower portions of the column where there was an increased area for friction and the centrifuge tests likely had higher frictional effects than the consolidometer. Frydman and Weisberg [1991] also reported data showing swell in the center of the centrifuge samples (by gamma-ray scans) was larger than swell on the sides (by photograph). The differences were largest near the base supporting the large effect side friction may have had. A graph from the report comparing swell in the center against swell at the sides is included as Figure 2.6.

Frydman and Weisberg [1991] also measured the advance of the water front through the centrifuge samples using electrical resistance transducers between each layer. As the moisture front hit the transducers the resistance would drop significantly and the moisture front could be located. The theoretical rate of advance of the wetting front was given by:

$$v = dh/dt = K\frac{N(h + H_0) + \alpha\phi}{n'h} \tag{2.22}$$

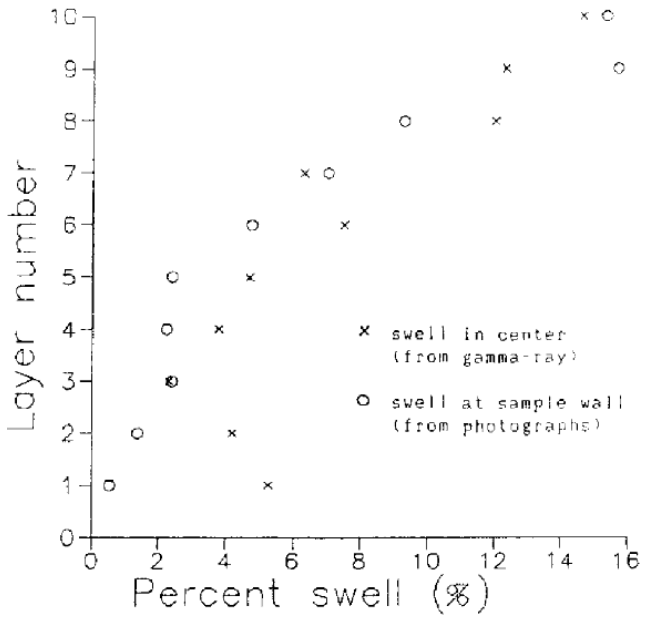

Figure 2.6: Swell along sample height (Frydman and Weisberg [1991])

where K is the coefficient of permeability of the wet soil, H_0 is the height of water head, h is the distance the wetting front has advanced, α is a coefficient between 0 and 1, ϕ is the suction at the wetting front, n' is the effective porosity, and N is the centrifugal acceleration.

In a comparison between measured data and the theoretical rates, Frydman and Weisberg [1991] concluded that flow was dominated by the pressure and elevation head ($N(h + H_0)$) and the suction ($\alpha\phi$) played little to no role. A decrease in hydraulic conductivity was found with time that was independent on the g level. The decrease was found to be dependent on time and not affected by the depth the wetting front had reached.

Gadre and Chandrasekaran [1994] performed centrifuge swell tests on black-cotton soil found locally to the authors in India. The clay had a liquid limit of 71%, a plastic limit of 32%, and a shrinkage limit of 10%. The soil is a Fat Clay, CH, by

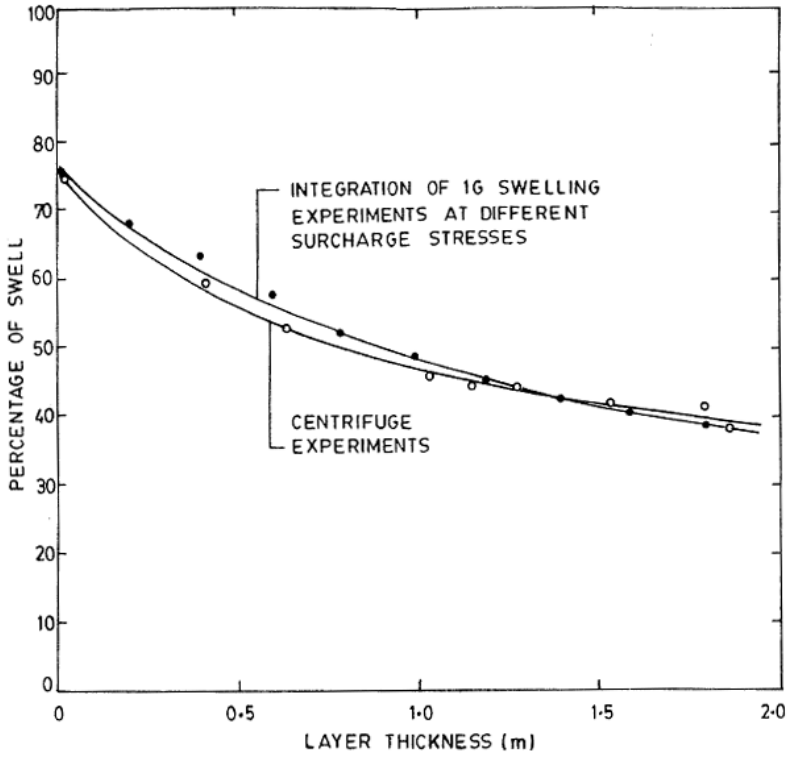

Figure 2.7: Stress-swell Relation of Black Cotton Soil (Gadre and Chandrasekaran [1994])

ASTM classification. Testing focused on solely the swelling of the clay and used 12.5 mm tall samples in a modified consolidation ring. Water was supplied to the base of the sample and swell was measured in flight by a LVDT placed on a porous disc on top of the sample. Little information was provided on the experimental procedures and analysis centrifuge stresses. The stress-swell relation (Fig. 2.7) found in the centrifuge was nearly identical to that found by standard free swell test. Swelling vs. time was reported, although no comparison was shown with that of 1g testing.

Chapter 3

Soil Characterization

The expansive soil used in this research study is a clay shale from the Eagle Ford formation. The clay had been excavated and processed for previous studies at the University of Texas (Kuhn [2005]) and was known to be highly expansive. The soil was excavated in Round Rock, Texas and air dried according to ASTM D 698-00a. The soil was then crushed until passing a #10 sieve. The soil characterization of the Eagle Ford clay was performed by Jeffrey Kuhn in work on his masters thesis. As the clay being used in this research study came from the same batch previously characterized, additional testing of index properties was not necessary.

3.1 Index Parameters

The Eagle Ford clay was reported to have a liquid limit of 88%, plastic limit of 39%, and shrinkage limit of 18%. The plasticity index is 49%. This classifies the soil as a highly plastic, fat clay (CH) according to USCS classifications and an A-7-5 soil according to AASHTO classifications. The specific gravity was reported as 2.74 and saturated hydraulic conductivity of 8.9×10^{-8} cm/s. Table 3.1 summarizes the

Table 3.1: Properties of Eagle Ford Clay (Kuhn [2005])

Test	Index Parameter	Value	ASTM Standard
Specific Gravity	Specific Gravity, G_s	2.74	D 845-02
Atterberg Limits	Liquid Limit, LL	88	D 4318
	Plastic Limit, PL	39	D 4318
	Shrinkage Limit, SL	18	D 4943
Particle Size Analysis	% Passing 0.075 mm (# 200 Sieve)	97	D 422-63
	% Passing 0.002 mm	76	D 422-63
Standard Proctor Compaction	Optimum water content, %	24	D 1557
	Maximum dry unit weight, $\gamma_{d\,max}$ (kN/m^3)	15.2	D 1557
Modified Proctor Compaction	Optimum water content, ω_{opt} (%)	14	D 698
	Maximum dry unit weight, $\gamma_{d\,max}$ (kN/m^3)	17.8	D 698
Hydraulic Conductivity of Saturated Soil	Hydraulic conductivity of Saturated Soil, K_{sat} (cm/s) (ω = 24%; γ_d= 15.2 kN/m3)	8.9×10^{-8}	D 5084

characterization of the Eagle Ford clay.

3.2 Compaction

Standard and modified proctor testing was completed in accordance with ASTM D 698-00a and ASTM D 1557-02. The maximum standard proctor density was reported to be 15.2 kN/m^2 (97.5 pcf) at 24% water content. The maximum modified proctor density was reported as 17.8 kN/m^2 (114 pcf) at 13% water content. The moisture density curves are included in Fig. 3.1.

3.3 Grain Size Distribution

A hydrometer test (ASTM D 422-63) was performed on the processed Eagle Ford clay. The resulting reported grain size distribution is included as Fig. 3.2. The hydrometer analysis showed 97% finer than a #200 sieve and 74% clay content (finer than .002 mm). Based on the clay content and plasticity index the activity ratio is 0.66.

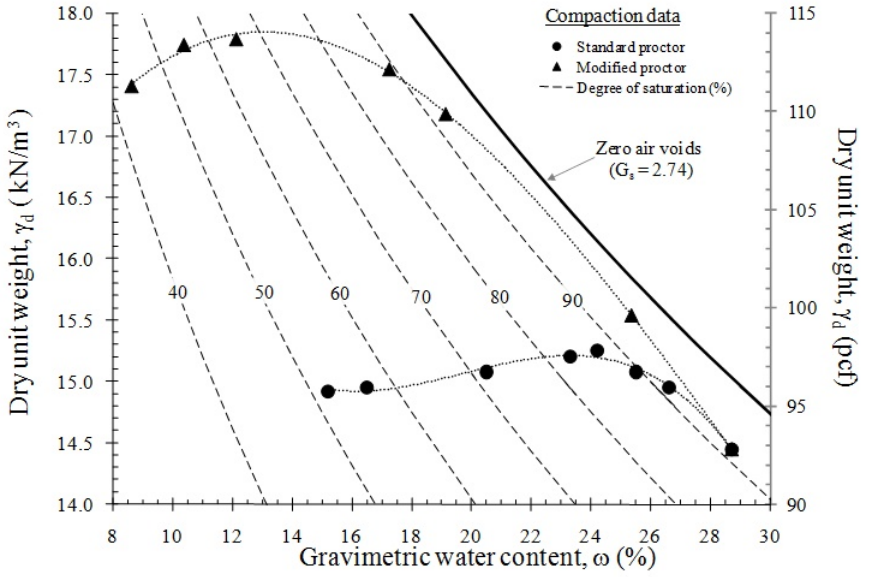

Figure 3.1: Compaction curve of Eagle Ford clay (Kuhn [2005])

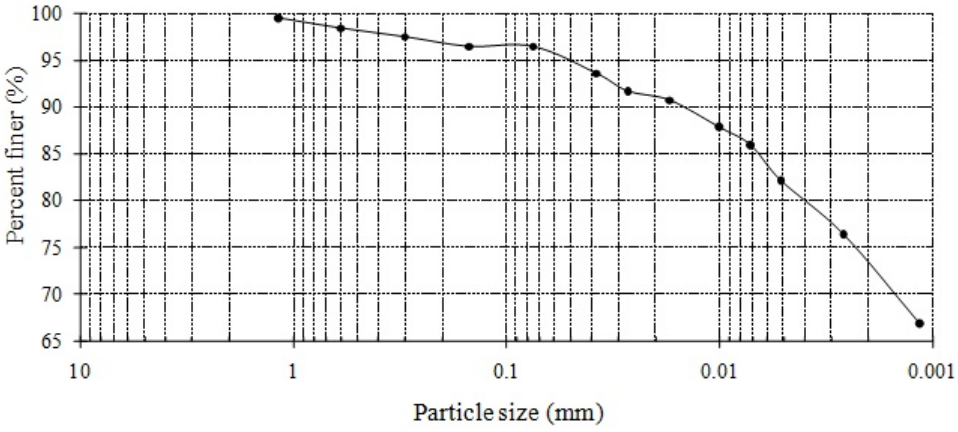

Figure 3.2: Grain size distribution of Eagle Ford Clay (Kuhn [2005])

Table 3.2: Predicted Swell of Eagle Ford Clay

Relation	Predicted Swell
Vijayvergiya & Ghazzalay	17.4%
Nayak & Christensen	26.4%
McDowell (PVR)	8%* (11.2%)
Rao et al.	6.2-15.2%

* at 1 psi overburden pressure (corrected to free swell)

Property	Value
Dry Unit Weight	97.5 pcf
Clay Content	74%
Water Content	24%
Liquid Limit	88%
Plasticity Index	49%

3.4 Correlations

Using the index properties listed in Section 3.1 the predicted swell was calculated using the relationships presented in Section 2.1.3. The resulting swell predictions are listed in Table 3.2 along with the values of index properties used. For the swell relation by Rao et al. [2004] a FSI range of 150-300 was used as one was not experimentally found. This range of FSI represents a clay with a "high" to "very high" degree of expansion. The value in parenthesis for the PVR prediction was corrected to a free swell pressure using the PVR procedure (Equation 2.4).

Even neglecting the relation by Rao et al. (as the FSI was estimated), the correlations show a wide range in predicted swell (11.2-26.4%). This agrees with the opinion of the researcher that swell predictions are generally poor and direct measurement is desirable.

Table 3.3: Free Swell Testing

Stress (psf)	Stress (kPa)	Swell (cm)	Final Height (cm)	Swell (%)
125	16	0.150	-	15
250	12	0.101	1.166	9.44
500	24	0.108	1.161	10.25
1000	48	0.068	1.074	6.74
4000	192	0.014	1.052	1.32

3.5 Free Swell Tests

A set of free swell tests were performed to evaluate the expansive properties of the Eagle Ford clay. Tests were performed between 125psf and 4000psf. The samples were compacted in a consolidation cell (2.5 inch diameter) to a height of one centimeter at optimum water content and maximum standard proctor density. The stress was then applied and consolidation was allowed. Once completed the samples were inundated with water and swell was measured over time by a dial gage indicator and a linear variable differential transformer (LVDT). Once swelling was completed the samples were drained and then the overburden pressure removed. The final height of the samples was then recorded.

The resulting heights and swells are recorded in Table 3.3. Swelling values were calculated using the final height and deflection except for the 125 psf where the sample dried before removal from the consolidation cell. This swell was calculated using the measured deflection and the target initial height of one centimeter. The swell over time measured by an LVDT is included in Fig. 3.3.

A best fit logarithmic relation was fit through the data points and the resulting coefficients were included in Table 3.4. The relation is plotted in Fig. 3.4.

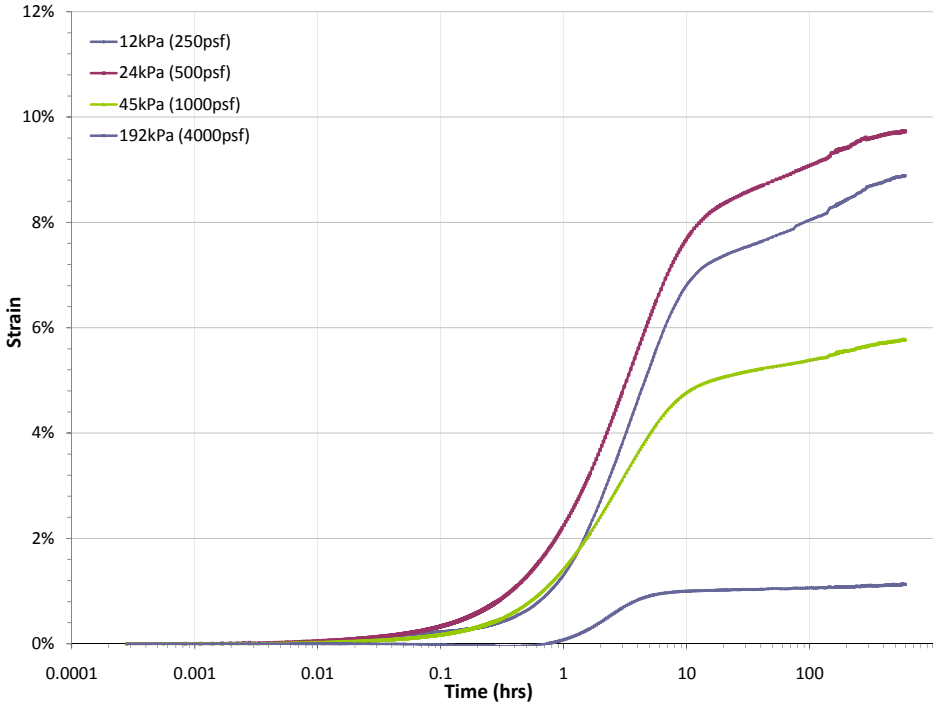

Figure 3.3: Swell Over Time

Table 3.4: Swell-Stress Relation (%-kPa)

Swell % = $Aln\sigma' + B$	
A	-3.635
B	20.598

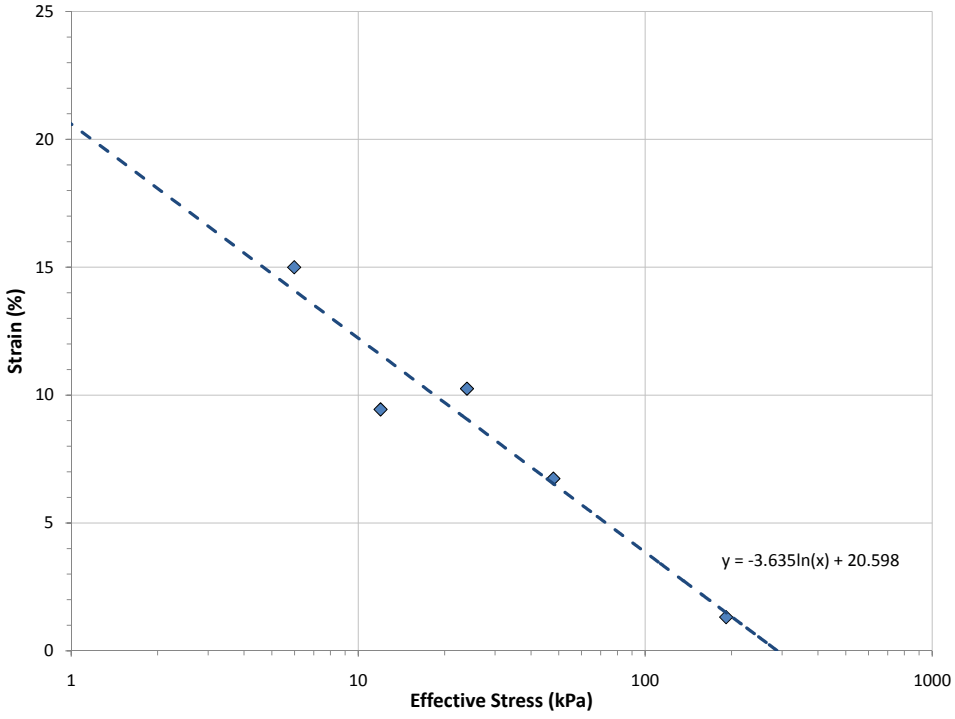

Figure 3.4: Swell Relation

Chapter 4

Equipment and Testing Procedure

4.1 Testing Equipment

The centrifuge used in this research study is a Damon / IEC centrifuge. It is the discontinued "IEC EXD" model which is floor mounted centrifuge used for a variety of purposes. It contains four hangers that hold freely swinging aluminum centrifuge cups. The setup of the centrifuge is fairly customizable as the contents of the centrifuge cups can be altered to fit requirements of different tests. Plastic permeameter cups that fit inside the centrifuge cups were designed and manufactured specifically for this research. The main components of the centrifuge are discussed individually in Sections 4.1.1-4.1.4. The centrifuge can be seen in Fig. 4.1

The centrifuge speed is controlled by a power setting knob on the side of the base. The power levels range from 0-100 and correlate with a power level for the electric motor. This causes the same power level to result in different rotational velocities depending on the mass of the test specimens. This is further discussed in Section 4.2.6.

The testing setup involves ponding water on top of a compacted soil sample

Figure 4.1: IEC EXD Centrifuge (pen resting on hanger for reference)

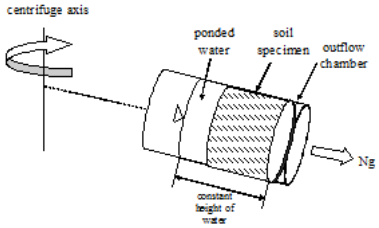

Figure 4.2: Centrifuge Test Setup

and spinning the sample at high g levels. The increased g level forces the water through the sample at an accelerated rate promoting the swelling of the clay. A simplified diagram of the test setup is shown as Fig. 4.2.

4.1.1 Centrifuge Cup

The centrifuge cups (Fig. 4.3) hang from the spinning centrifuge arms and were provided with the centrifuge and have not been significantly altered. The holders have an inner diameter of 2.5 inches and a usable inside depth of 4.5 inches. The

Figure 4.3: Centrifuge Cup

base of the specimen holder has a small vent hole to allow air and water outflow. When in flight the distance from the base of a sample to the center of rotation in the small centrifuge is 6.5 inches.

4.1.2 Permeameter Cup

The permeameter cups (Fig. 4.4) fit inside the centrifuge cups and have an outside diameter of 2.49 inches and a depth of 4.5 inches. The cups have an inside diameter of 2.25 inches at the top that is reduced to 1.855 inches one inch from the base of the cups to form a ledge that allow a porous plate to support soil samples. The base of the cup is removable and is used as a liquid collection system. Outflow can be measured accurately by measuring the increase in weight of the collection cup. A small air vent connects the collection cup to the area above the sample to allow equal air pressures above the ponded water and on the bottom of the sample.

4.1.3 Porous Supporting Plate

The porous supporting plate (Fig. 4.5) sits on top of the ledge in the permeameter cup and creates a surface to place specimens. The plate contains 1/32″ holes that

Figure 4.4: Permeameter Cup

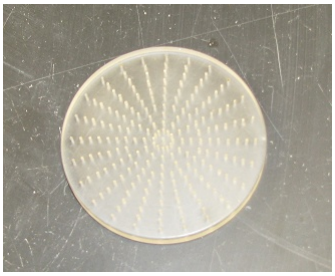

Figure 4.5: Porous Supporting Plate

allow water to flow freely from the base of the specimen. To avoid soil migration a filter paper is placed between the porous plate and the soil specimen.

4.1.4 Permeameter Cap

A rubber permeameter cap (Fig. 4.6) fits inside the top of the permeameter cup and prevents excessive evaporation while testing. The rubber cap provides an air tight seal once the centrifuge is in flight.

Figure 4.6: Permeameter Cap

4.2 Centrifuge Testing Procedure

A testing procedure was developed for the swell testing of expansive clays in the centrifuge. This procedure is detailed in the following sections.

4.2.1 Soil Preparation

Processed soil was prepared at optimum water content ($\omega_{opt} = 24\%$) by adding the appropriate water mass with the use of a spray bottle. Details on the soil processing can be found in Chapter 3. Soil was prepared in batches ranging from two to five kilograms. An attempt was made to evenly distribute the water mass throughout the soil. Once the water mass had been added the soil mixture was stored in an air tight plastic container for at least 48 hours.

Water contents were taken periodically of the prepared soil and was considered acceptable if the water content was within 1% of optimum. The threshold of 1% was chosen based on results from Rao et al. [2004] predicting less than 0.5% fluctuation in swell from this range of water contents. In general the initial water content used in testing ranged from 23.5% to 24%.

4.2.2 Equipment Preparation

Prior to every test the centrifuge equipment was cleaned and dried. Pressurized air was blown through the porous supporting disk when needed to remove soil particles and ensure free drainage. A porous supporting disk was inserted onto the ledge in the permeameter cup and the inside of the permeameter cup was lubricated with vacuum grease where soil would be in contact with the cup. Grease was included 1 cm higher than the level the soil was expected to be compacted to account for swelling. A filter paper was placed on top of the porous disk to prevent loss of fines. The mass of the permeameter cup (including porous disk, filter paper, and grease) and its removable base were recorded after cleaning and lubrication.

4.2.3 Soil Compaction

Soil compaction was accomplished using a kneading compactor (Figure 4.7) that allows a constant pressure to be exerted on the soil during compaction. The soil was compacted in one centimeter lifts as follows:

- The distance from the base of the sample to the top of permeameter cup was measured.
- The appropriate soil mass for a single lift was poured into the permeameter cup. It was found to be best to use a funnel (or rolled up sheet of paper) to prevent the soil from sticking to the lubricated sides of the permeameter cup.
- The soil was initially compacted by hand (using a finger to press down the soil) until the soil structure was strong enough to resist the kneading compactor foot without extensive mass movement.

Figure 4.7: Kneading compactor

- The kneading compactor foot was then used to apply pressure to the surface of the soil. The compactor foot was first used around the edges of the sample and then in the center.

- Once the sample height appeared to be close to the desired height, a caliper was used to measure from the top of the permeameter cup to the top of the compacted soil. The sample height was calculated as the difference of this measurement and the previous measurement from the base of the sample to the top of the permeameter cup. This measurement was taken on four sides of the sample and in the center.

- If needed additional pressure was applied to the top of the sample until the desired height was achieved.

This process was repeated for each lift until the final sample height was achieved. A filter paper was inserted on top compacted soil after the final lift.

4.2.4 Measurement of sample height

Several methods were explored to accurately determine the height of the soil sample. Initially, as with measuring for compaction height, the sample height was found by measuring down from the top of the permeameter cup to the soil. This

measurement was taken at four sides and averaged to find the sample height. However this method was found to not provide accurate and consistent results, mainly a result of the uneven surface of the compacted soil sample. As the testing plan included sample heights of as low as one centimeter and strains were expected on the order of 10-20% errors greater than 2 mm (2% strain) were considered too high.

The final method used for measurement of sample height was as follows:

- The mass of the permeameter cup with compacted soil and filter paper was recorded.
- Approximately 2 cm of water was poured gently on top of the sample and the new mass recorded.
- The distance from the base of the sample to the top of the water was measured. The base of the meniscus is used as an even surface to measure to (provided the permeameter cup is sitting level).
- The water was then suctioned off and the sample height was calculated from the measured distance corrected by the volume of water suctioned off.

In order to increase the accuracy of the calculated final swell, initial and final sample heights were measured twice and the average of the two was used. This method of height measurement, its accuracy and other consideration are discussed further in Chapter 6.

4.2.5 Application of overburden pressure and water head

Overburden pressure was provided to the samples by metal washers placed on top of a second porous supporting disk on top of the sample. The washers were used

Figure 4.8: Washers for overburden pressure

in sets of three with the intention of keeping the weights centered on the porous disk. Single washers were originally used but uneven swelling had been observed with the weight resting toward the low side of the cup. A set of three washers is large enough that no major shifting can occur. A photo of three washers as they are used in testing is included as Fig. 4.8.

The water head was applied to the sample by pouring the appropriate mass of water on top of the sample. A head of two centimeters of water was used as the standard for testing. Considering the hydraulic conductivity of the Eagle Ford clay, two centimeters of water was sufficient that tests could be run for several days without refilling the water. The effects of varying water heads are discussed in Chapter 6.

4.2.6 Centrifugation

The permeameter cups were placed inside the centrifuge cups and hung in the centrifuge. The rubber permeameter caps were placed in the tops of the permeameter cups to prevent excessive evaporation. Samples were flown in sets to counterbalance each other in the centrifuge. If masses of the two samples being flown together varied greater than 5g washers were inserted in the centrifuge cup below the permeameter cup to increase the mass.

For the final testing procedure, the centrifuge power level was set and increased until the desired rotational velocity measured by laser site was met. The rotational velocity was also recorded before stopping the centrifuge. It was initially thought that a power level could be found that corresponded to a g level and the centrifuge set to the power level when testing at that g level. However it was discovered that the centrifuge rotational velocity was not constant with respect to power level. As a result some of the initial testing uses an estimated g level (from power level) rather than one directly measured. The effects of this are discussed in Chapter 6.

4.2.7 Test Duration

In traditional free swell testing the test duration is not a set time and tests are run until swelling is completed. Readings are taken during the test (by LVDT or dial Gage) and are plotted to determine if swelling has completed. However in the centrifuge used for this research study no in flight data can be acquired. Measuring the sample height requires the centrifuge to be stopped resulting in the sample experiencing stresses of the natural 1g environment.

This reduction in stress allows further swelling of the sample. This could

be avoided by the addition of in flight data acquisition however the size of the centrifuge prohibited this addition. There was simply not enough room on top of the sample to mount a LVDT. The centrifuge also does not include a slip ring stack to provide power to the LVDT further complicating the issue even if an LVDT was able to fit. Furthermore one of the goals of this study was to provide a simple, economical method for the measurement of swell. Even if some sort of in flight data acquisition system was manufactured, it would increase the cost of the centrifuge to a point where it would likely not be economical in comparison to a traditional free swell test.

Therefore it was decided that a pilot test would be performed for each sample height. These tests would take measurements throughout the test with the sole purpose of determining when swelling completed. These pilot tests indicated that swelling for a 1 cm-high sample completed after approximately one day. Two centimeter high samples completed after two days. It was decided that 1 cm-high samples should be flown for two days and 2 cm-high samples for three days. This allowed samples to fly for the duration of the test without interruption at the desired increased g level. The samples were removed at the end of the test duration and the final heights were measured. This minimized the time the samples were in a 1g environment. Further discussion on the effect of measuring sample height after the centrifuge has stopped can be found in Chapter 6.

4.2.8 Measured Variables

The three variables that were measured throughout the test were the mass of the permeameter cup, the mass of the outflow chamber, and the distance from the base of the water meniscus to the base of the sample. Using these variables it was pos-

sible to calculate sample height, unit weight, void ratio, inflow, and outflow.

In order to calculate these properties the mass of the permeameter cup and outflow chamber were taken prior to testing. These masses were also measured before the cup was put in the centrifuge and as soon as it was taken out. The mass of the permeameter cup was also taken after the water had been suctioned off. Table 4.1 lists the calculated properties and their equations.

After completion of tests, the samples were removed from the permeameter cups and oven dried to obtain an average water content. Two centimeter samples were generally cut in half and water content taken on both portions. A handful of tests had water contents taken from $\frac{1}{4}$ cm section.

4.3 Typical Results

Centrifuge tests were run in three general sets. The first set of tests that were preliminary tests without a definitive testing procedure. A graph of several of these tests is included in Fig. 4.9a. These tests were run for over a week with data collected periodically throughout the test. The main purpose of these tests were to familiarize the researchers with the testing equipment.

The second set of tests were run using the testing procedure previously discussed. The focus of these tests was to determine, before proceeding with rigorous testing, if there was a correlation between the centrifuge tests and standard 1g free swell tests. These tests were run on 1 cm-high samples and data was recorded at approximately 24 and 48 hours. A test set is shown in Fig. 4.9b.

The final test set was conducted for the purpose of acquiring data sets for analysis of repeatability and parametric evaluation of the effect of g level and sample height. As per the testing procedure, tests with sample heights of one centime-

Table 4.1: Calculated Properties for Centrifuge Samples

Property	Equation	Variables
Sample Height	$H_i = \left(L_i - \frac{M_{pc1,i} - M_{pc2,i}}{\gamma_w \pi R^2}\right)$	L_i Distance from base of meniscus to base of sample, test point i $M_{pc1,i}$ Mass of permeameter cup with water head, test point i $M_{pc2,i}$ Mass of permeameter cup after water head suctioned, test point i γ_w Unit weight of water R Interior radius of permeameter cup
Unit Weight	$\gamma_i = \frac{M_{pc2,i} - M_{pci}}{\pi R^2 H_i}$	$M_{pc2,i}$ Mass of permeameter cup after water head suctioned, test point i M_{pci} Initial mass of permeameter cup (before soil compaction) R Interior radius of permeameter cup H_i Sample height, test point i
Outflow Mass	$OF_m = M_{of,i} - M_{of,i-1}$	$M_{of,i}$ Mass of outflow chamber, test point i $M_{of,i-1}$ Mass of outflow chamber, test point $i-1$
Inflow Mass	$IF_m = \left(M_{pc3,i-1} - M_{pc2,i-1}\right) - \left(M_{pc1,i} - M_{pc2,i}\right)$	$M_{pc3,i-1}$ Mass of permeameter cup after water head reapplied, test point $i-1$ $M_{pc2,i-1}$ Mass of permeameter cup after water head removed, test point $i-1$ $M_{pc1,i}$ Mass of permeameter cup with water head, test point i $M_{pc2,i}$ Mass of permeameter cup after water head removed, test point $i-1$

ter were run for two days and and sample heights of two centimeters for three days. Data was only taken for the initial and final conditions. Figure 4.9c includes sets of 2 cm-high samples flown three different g levels. The initial void ratio is plotted versus the final.

The three plots seen in Fig. 4.9 represent the range of typical test results seen in the centrifuge testing program. The complete testing program and results are included in Chapter 5.

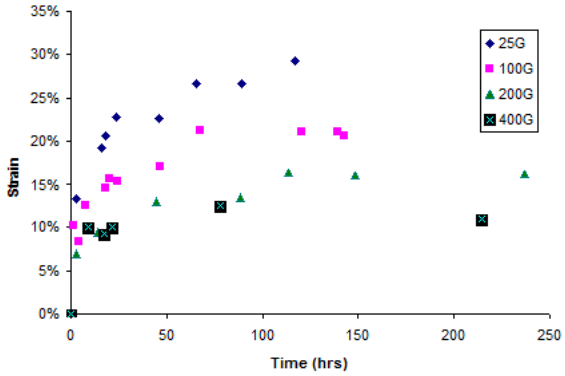

(a) Preliminary testing

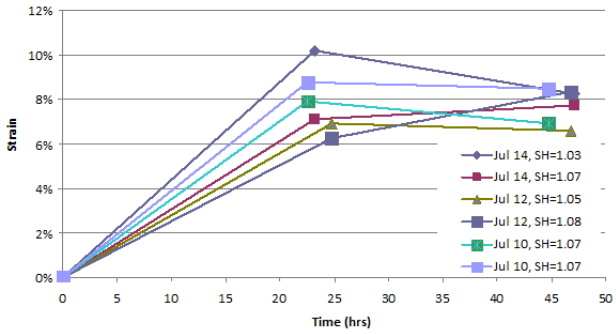

(b) Initial testing

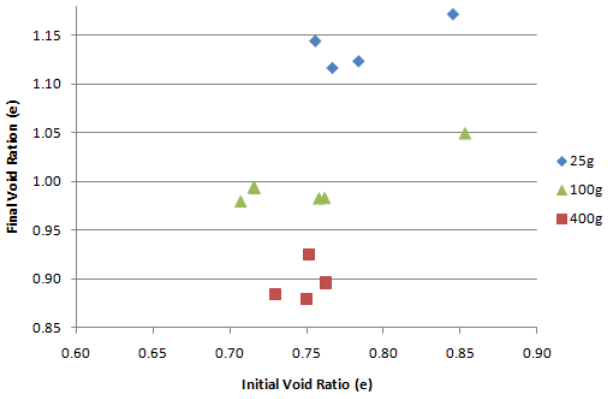

(c) Finalized tests

Figure 4.9: Typical Centrifuge Test Results

Chapter 5

Testing Program and Results

5.1 Testing Program

Thirty six tests were performed in the main testing program. These tests were selected in an attempt to evaluate the effects of g level and sample height. The initial testing program concentrated on 1 cm-high samples. However after sixteen tests were performed, the scatter of the results was found to be too high and the test program was revised. The revised testing program focused on tests of 2 cm-high samples at g levels of 25, 100, and 400. Two tests with increased overburden pressures were also included. Water head was chosen to be constant for all tests as discussed in Section 4.2.5. The scope of the testing program is linsted in Table 5.1. Tests above the row denoted "Testing Program Revised" are from the initial testing plan.

Table 5.1: Testing Program

Target G Level	Water Head (cm)	Sample Height (cm)	Overburden (g)	Samples
100	2	1	20	2
100	2	2	20	2
100	2	1	12	8
200	2	1	12	8
Testing Program Revised				
25	2	2	12	4
100	2	2	12	6
400	2	2	12	4
100	2	2	40	2

5.2 Results

The tests listed in Table 5.1 were completed and the results are included in Tables 5.2-5.4. Table 5.2 includes the results from pilot tests on 1 cm-high and 2 cm-high samples used in order to determine testing duration. Table 5.3 includes the results from the tests performed before the testing program was revised and are all on 1 cm-high samples. The results from the revised program on 2 cm-high samples are included in Table 5.4.

The results presented in this section are the compaction dry density, initial height, and final height. The initial and final heights were determined according to procedures discussed in Section 4.2.4 and are the average of two readings. The compaction dry density was calculated using the initial height, mass of wet soil, and target water content. Soil mixes were considered acceptable if within +/- 1% of target water content (Section 4.2.1) resulting of errors in the calculated dry density of up to 0.01 g/cm^3.

It should be noted that the 100g and 200g testing program was completed before it was found that the g level fluctuated widely at a constant power level. In

Table 5.2: Pilot Tests For Duration

Test ID	G level	Water Head (cm)	Overburden (g)	Compaction Dry Density (g/cm^3)	Initial Height (cm)	Final Height (cm)
01	105	2	20	1.49	2.08	2.31
02	105	2	20	1.61	1.93	2.21

the tests listed as 105g and 200g, the centrifuge was set to a constant power level that had been determined to result in the correct rotational velocity and the g level was not measured directly at the end of testing. For the remaining tests, rotational velocity was measured directly and the calculated g level is listed.

The data (excluding pilot tests) has also been displayed in Figs. 5.1 and 5.2 grouped by sample height. The initial void ratio is plotted versus the final void ratio. The large amount of scatter found in tests of 1 cm-high samples can be seen in Fig. 5.1 where there is little difference in final void ratio between the 100g and 200g tests. For testing performed on 2 cm-high samples (Fig. 5.2) there are visible trends between final void ratio and g level. An increase in final void ratio is also seen with increasing initial void ratio.

Table 5.3: One Centimeter Testing Program

Test ID	G level *	Water Head (cm)	Overburden (g)	Compaction Dry Density (g/cm^3)	Initial Height (cm)	Final Height (cm)
05	200	2	12	1.48	1.05	1.23
06	200	2	12	1.53	1.02	1.18
07	200	2	12	1.56	1.03	1.17
08	200	2	12	1.55	1.00	1.18
09	200	2	12	1.53	1.02	1.19
10	200	2	12	1.47	1.05	1.16
11	200	2	12	1.54	1.00	1.11
12	100	2	12	1.56	0.99	1.22
13	100	2	12	1.55	1.01	1.17
14	100	2	12	1.55	0.98	1.19
15	100	2	12	1.58	0.97	1.20
16	100	2	12	1.60	0.96	1.16
17	100	2	12	1.63	0.97	1.16
18	100	2	12	1.54	0.99	1.15
19	100	2	12	1.54	1.00	1.20

* g level estimated by power level

Table 5.4: Two Centimeter Testing Program

Test ID	G level	Water Head (cm)	Overburden (g)	Compaction Dry Density (g/cm^3)	Initial Height (cm)	Final Height (cm)
20	105*	2	12	1.61	1.93	2.24
21	105*	2	12	1.60	1.94	2.25
22	105*	2	12	1.56	1.99	2.24
23	105*	2	12	1.60	1.94	2.25
24	105*	2	12	1.56	2.00	2.26
25	105*	2	12	1.48	2.11	2.33
26	29	2	12	1.54	2.01	2.39
27	29	2	12	1.55	2.01	2.41
28	36	2	12	1.56	1.98	2.42
29	36	2	12	1.49	2.10	2.47
30	340	2	12	1.55	1.97	2.12
31	340	2	12	1.58	1.96	2.14
32	360	2	12	1.56	1.98	2.18
33	360	2	12	1.57	1.98	2.12
34	105	2	40	1.58	1.95	2.20
35	105	2	40	1.57	1.97	2.19

* g level estimated by power level

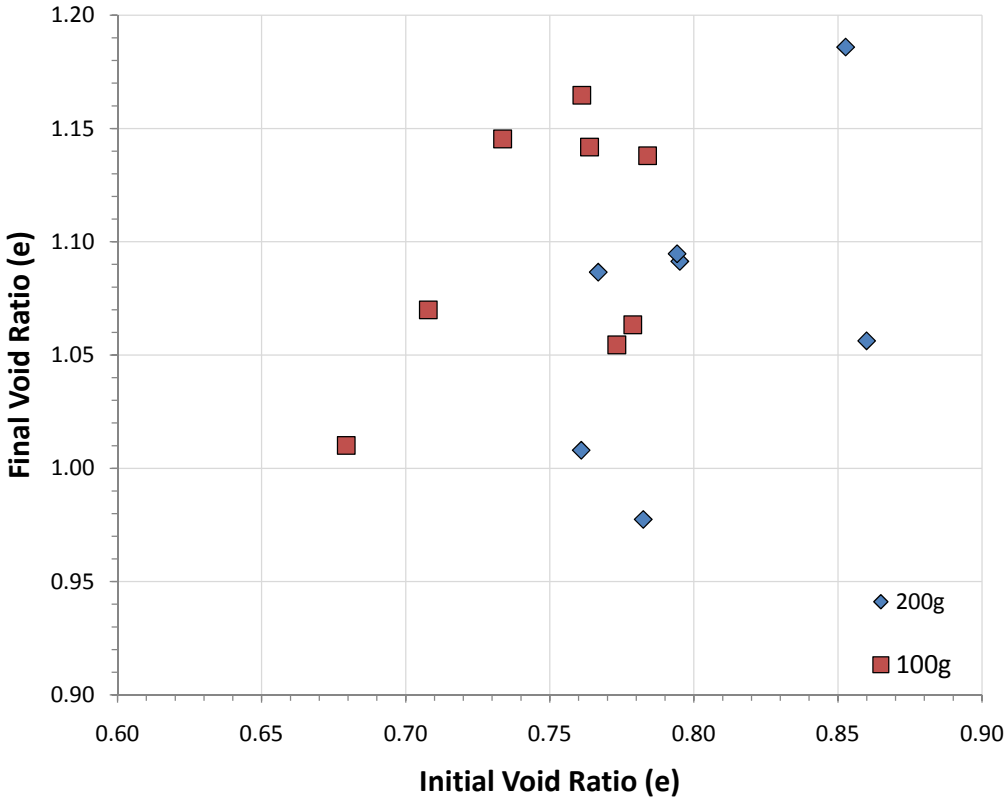

Figure 5.1: One Centimeter Tests

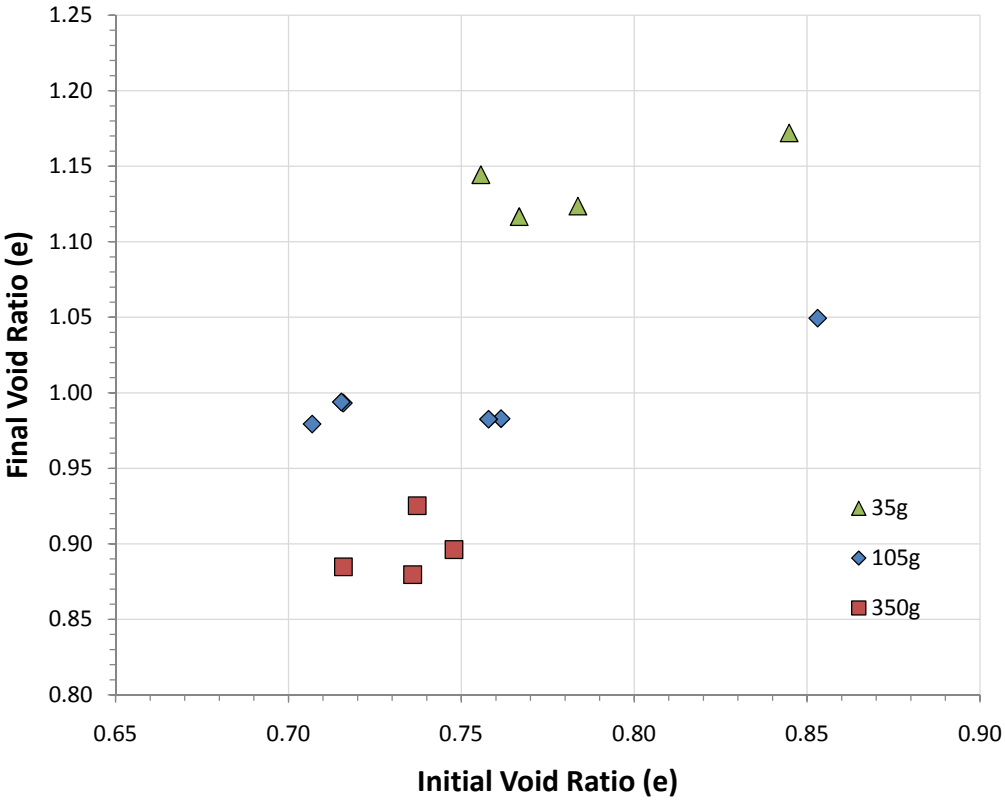

Figure 5.2: Two Centimeter Tests

Chapter 6

Analysis

6.1 Measurement Errors

6.1.1 Sample Height

The sample height was calculated according to the procedure discussed in Section 4.2.4. The procedure requires that the sample height be calculated as follows:

$$H = \left(L - \frac{M_{pc1} - M_{pc2}}{\gamma_w \pi R^2} \right) \tag{6.1}$$

where M_{pc2} is the mass of the permeameter cup and soil, M_{pc1} is the mass of the permeameter cup, soil, and ponded water, and L is the distance from the base of the sample to the base of the meniscus of the ponded water. These variables are measured twice at two water levels and the average is taken as the sample height.

One approach for determining the accuracy of the sample height measurement was to repeatedly measure a soil sample of constant height and determine the standard deviation from the set of measurements. However, as the soils tested in this project were expansive clays the soil sample would increase in sample height

Table 6.1: Data Set, $D = H_2$-H_1 (cm)

Initial Readings					Final Readings				
0.034	-0.039	-0.016	-0.007	0.002	-0.048	0.021	0.016	0.003	0.009
-0.010	-0.011	0.020	0.007	0.050	-0.025	0.025	0.024	0.004	0.036
-0.040	-0.029	-0.040	0.061	0.015	0.011	-0.034	-0.007	0.016	0.022
0.020	0.006	-0.006	0.020	0.000	0.018	0.025	0.022	0.009	0.026
0.026	-0.024	0.033	0.029	0.010	0.011	-0.011	0.000	0.032	-0.006
-0.023	0.037	0.000	0.022		-0.021	-0.003	-0.071	0.001	
-0.033	-0.012	-0.020	-0.037		0.006	0.010	0.013	0.025	
Average: 0.001					Average: 0.005				
Standard Deviation: 0.027					Standard Deviation: 0.023				

Standard Deviation: 0.025 (both)

over time even if perfect measurements were taken. Instead a data set was populated from differences of two measurements of height. This data was already available, as initial and final heights were taken twice for each test. The data set of the difference (D) between the two measurements (H_1,H_2) is included as Table 6.1. The average difference for the initial reading was 0.001 cm and 0.005 cm for the final readings. The positive average difference indicates a slight increase in sample height between measurements. The swell, however, is minor and would result in an error of approximately $\frac{1}{10}$ of a percent in strain of a 2 cm-high sample and corrections were not performed.

The standard deviation of the difference was related to the standard deviations of single measurements as:

$$\sigma_D = \sqrt{\sigma_{H_2}^2 + (-\sigma_{H_1})^2} = 0.025cm \tag{6.2}$$

where σ_D, σ_{M1} and σ_{M2} were the standard deviations of the difference, measurement one, and measurement two respectively. Assuming that the standard deviation of both measurements were equal (same procedure) they were calculated as:

Table 6.2: Mass Measurement Set (grams)

Measured Masses (20)				
211.11	211.12	211.11	211.10	211.11
211.13	211.11	211.11	211.11	211.12
211.12	211.12	211.11	211.11	211.11
211.11	211.12	211.11	211.12	211.12
Average:			211.11	
Standard Deviation:			.007	

$$\sigma_{H_{1,2}} = \sqrt{\frac{1}{2}\sigma_D^2} = 0.018cm \tag{6.3}$$

The standard deviation of the sample height (the average of two measurements), σ_H, was then calculated using:

$$\sigma_{H_{ave}} = \sqrt{(0.5\sigma_H)^2 + (0.5\sigma_H)^2} = 0.013cm \tag{6.4}$$

6.1.2 Mass

In order to determine the accuracy of the measured masses, twenty readings were taken of a permeameter cup with compacted soil. The average measured mass was 211.11 grams with a standard deviation of 0.07 grams. The readings are included in Table 6.2.

It was unlikely that the mass of the measured permeameter cup varied over the measurements and therefore the actual mass was considered constant and the standard deviation was solely due to errors in measurement. The measured masses appeared the be normally distributed and were modeled as:

$$M_m\left(M, .007\right) = M + E\left(0, .007\right) \tag{6.5}$$

Table 6.3: Standard Deviations Based on Measurement Error

Property	Method	Standard Deviation (1 cm Sample)	Standard Deviation (2 cm Sample)
Mass of Soil	Standard	0.01g	0.01g
Mass of Solids	Standard	0.008g	0.008g
Void Ratio	Monte Carlo	0.032	0.016
Dry Density	Monte Carlo	0.028 g/cm^3	0.014 g/cm^3
Strain	Monte Carlo	2.84%	1.33%

where $E()$ is a normally distributed model of the error in mass measurement.

6.1.3 Effect of Errors

The errors in measurement from Sections 6.1.1 and 6.1.2 were applied to properties likely to be calculated. A summary of the standard deviations expected in these properties solely from measurement errors is included in Table 6.3. Monte Carlo simulations were performed to estimate the standard deviation of properties with complex formulas. Further details on the calculation of each property are included in Sections 6.1.3.1-6.1.3.5.

The most important detail from the analysis on the effect of measurement error is the increased effect the errors have on properties of shorter samples. Because the measurement errors were a discrete amount, the percent effect was larger on the 1 cm-high samples than on the 2 cm-high samples. This was reflected in the testing results. Figure 6.1 includes data of initial and final void ratios at varied g level separated by sample height. The results from the 1 cm-high samples showed a wide range in both initial and final void ratio. The 100g and 200g tests were not distinguishable from one another based on final void ratio. However the 2 cm-high samples showed defined ranges in final void ratio based on g level. This was par-

tially due to the 1 cm-high samples being tested at a narrower range in g levels but the main source of scatter in the 1 cm-high samples was due to measurement error of sample height. The effects of measurement error caused twice as much scatter in readings on 1 cm-high samples than on 2 cm-high samples.

The scatter from measurement error in tests on 1 cm-high specimens was too high for any serious analysis and this was the cause for the revision in testing plan discussed in Chapter5. The completed tests on 1 cm-high samples were used in analysis of compaction however analysis of final results was completed solely on the more reliable tests of 2 cm-high samples.

6.1.3.1 Mass of Soil

The mass of soil was calculated as the difference between the measured mass of the permeameter cup and the measured mass of the permeameter cup and soil such that:

$$M_{soil,calc} = M_{pc+soil,measured} - M_{pc,measured} \tag{6.6}$$

The measured masses of soil were calculated taking into account the errors in mass measurement discussed in Section 6.1.2 as:

$$M_{pc+soil,measured} = M_{pc+soil} + E_{pc+soil}\,(0, .007) \tag{6.7}$$

$$M_{pc,measured} = M_{pc} + E_{pc}\,(0, .007) \tag{6.8}$$

Equations. 6.7 and 6.8 were substituted into 6.6 resulting in the the calculated mass of soil:

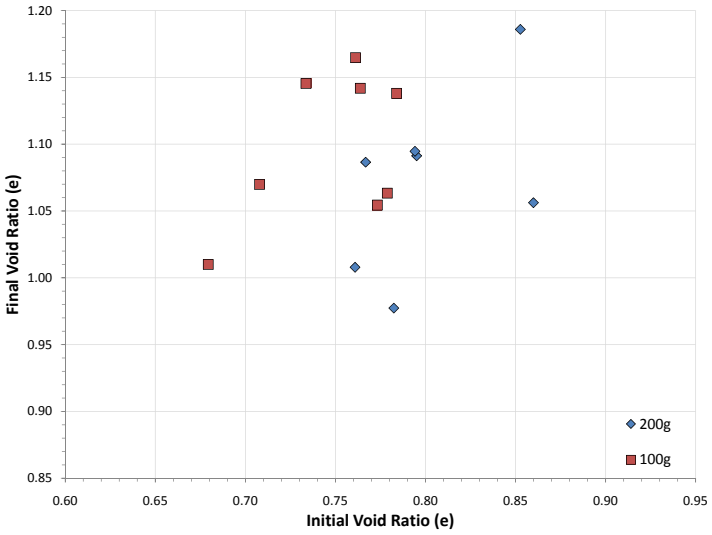

(a) 1 cm-high Samples

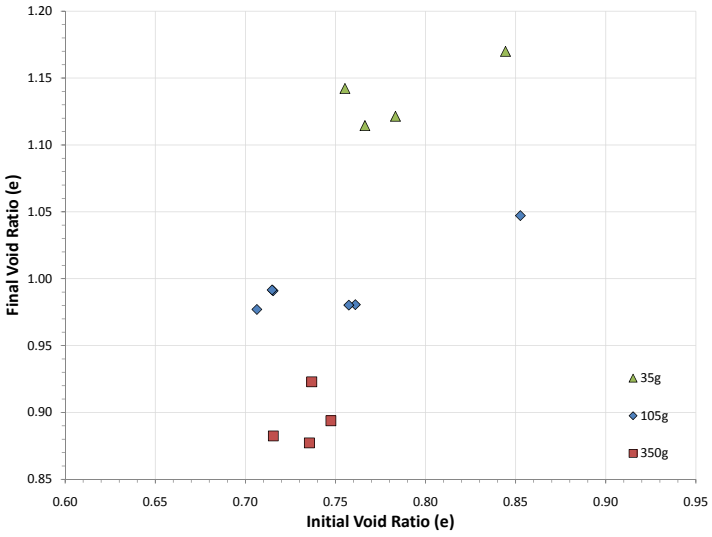

(b) 2 cm-high Samples

Figure 6.1: Scatter in results for different sample heights

$$M_{soil,calc} = M_{pc+soil} + E_{pc+soil}\,(0, .007) - M_{pc} - E_{pc}\,(0, .007) \tag{6.9}$$

The mass of the permeameter cup (M_{pc}) was subtracted from the mass of the permeameter cup and soil ($M_{pc+soil}$) in Eqn. 6.9 resulting in the mass of soil (M_s) such that:

$$M_{soil,calc} = M_{soil} + E_{pc+soil}\,(0, .007) - E_{pc}\,(0, .007) \tag{6.10}$$

The standard deviation of the calculated mass of soil due to measurement error was then calculated as:

$$\sigma_{M_{soil,calc}} = \sqrt{\sigma^2_{E_{pc+soil}} - (-\sigma_{E_{pc}})^2} = 0.01g$$

6.1.3.2 Mass of Solids

The mass of solids was calculated using:

$$M_s = \frac{M_{soil}}{1 + \frac{W_c}{100}} \tag{6.11}$$

where $W_c$is the water content as a percent. The target water content was 24% and was used in all calculations. The standard deviation for mass of soil was 0.01g (Section 6.1.3.1) resulting in a standard deviation of 0.008g for mass of solids.

6.1.3.3 Void Ratio

The void ratio was calculated using:

$$e = \frac{V_t - \frac{M_s}{G_s}}{\frac{M_s}{G_s}} \tag{6.12}$$

Table 6.4: Void Ratio Monte Carlo Summary

Void Ratio (e)			
M_s		normsinv(rand())$\sigma_{M_{soil,calc}} + \mu_{M_s}$	
H_{ave}		normsinv(rand())$\sigma_{H_{ave}} + \mu_{H_{ave}}$	
Iterations		10,000	
One Centimeter Sample		Two Centimeter Sample	
$\sigma_{M_{soil,calc}}$	0.01 g	$\sigma_{M_{soil,calc}}$	0.01 g
$\sigma_{H_{ave}}$	0.013 cm	$\sigma_{H_{ave}}$	0.013 cm
μ_{M_s}	49.3 g	μ_{M_s}	98.6 g
$\mu_{H_{ave}}$	1 cm	$\mu_{H_{ave}}$	2 cm
Standard Deviation	0.0317	Standard Deviation	0.0157
95% Confidence Interval	0.0304-0.0330	95% Confidence Interval	0.0151-0.0163

where;

$$V_t = \pi r^2 H_{ave} \tag{6.13}$$

A Monte Carlo simulation was performed in Excel where H_{ave} and M_s were modeled using normal distributions with independent random numbers. Formulas and values used in the Monte Carlo simulation are included in Table 6.4. Iterations were performed in sets of 1,000 with a total of 10 sets. Resulting standard deviations from each set were used to calculate a confidence interval of the average standard deviation for all iterations. The resulting standard deviation for void ratio of 1 cm-high samples was 0.0317 with a 95% confidence interval (+/- 2σ) of 0.0304-0.0330. The standard deviation for void ratio for 2 cm-high samples was 0.0157 with a 95% confidence interval of 0.0151-0.0163.

Table 6.5: Dry Density Monte Carlo Summary

Dry Density (γ_d)			
M_s		normsinv(rand())$\sigma_{M_{soil,calc}} + \mu_{M_s}$	
H_{ave}		normsinv(rand())$\sigma_{H_{ave}} + \mu_{H_{ave}}$	
Iterations		10,000	
One Centimeter Sample		Two Centimeter Sample	
$\sigma_{M_{soil,calc}}$	0.01 g	$\sigma_{M_{soil,calc}}$	0.01 g
$\sigma_{H_{ave}}$	0.013 cm	$\sigma_{H_{ave}}$	0.013 cm
μ_{M_s}	49.3 g	μ_{M_s}	98.6 g
$\mu_{H_{ave}}$	1 cm	$\mu_{H_{ave}}$	2 cm
Standard Deviation	0.0277	Standard Deviation	0.0137
95% Confidence Interval	0.0263-0.0294	95% Confidence Interval	0.0130-0.0144

6.1.3.4 Dry Density

A Monte Carlo simulation was also performed to determine the standard deviation of the dry density from measurement error. The dry density was calculated as:

$$\gamma_d = \frac{M_s}{V_t} \tag{6.14}$$

where V_t is determined according to Eqn. 6.13. The resulting standard deviation for dry density of a 1 cm-high sample was 0.0277 g/cm^3 with a 95% confidence interval (+/- 2σ) of 0.0263-0.0294 g/cm^3. The resulting standard deviation for dry density of a 2 cm-high sample was 0.0137 g/cm^3 with a 95% confidence interval of 0.0130-0.0144 g/cm^3. The Monte Carlo simulation properties are displayed in Table 6.5.

Table 6.6: Monte Carlo Summary For Strain

10% Strain			
H_{ave1}		normsinv(rand())$\sigma_{H_{ave1}} + \mu_{H_{ave1}}$	
H_{ave2}		normsinv(rand())$\sigma_{H_{ave2}} + \mu_{H_{ave2}}$	
Iterations		10,000	
One Centimeter Sample		Two Centimeter Sample	
$\sigma_{H_{ave1,2}}$	0.013 cm	$\sigma_{H_{ave1,2}}$	0.013 cm
$\mu_{H_{ave1}}$	1 cm	$\mu_{H_{ave1}}$	2 cm
$\mu_{H_{ave2}}$	1.1 cm	$\mu_{H_{ave2}}$	2.2 cm
Standard Deviation	2.78	Standard Deviation	1.33
95% Confidence Interval	2.64-2.82	95% Confidence Interval	1.24-1.42

6.1.3.5 Strain

A Monte Carlo simulation was also performed to determine the standard deviation of the strain from measurement error. The strain was calculated as:

$$S\% = \frac{\frac{H_{ave2}}{2} - \frac{H_{ave1}}{2}}{\frac{H_{ave1}}{2}} \times 100 \tag{6.15}$$

Initial and final sample heights were selected for 1 cm-high and 2 cm-high centimeter samples to be representative of strains generally seen in the centrifuge. The resulting standard deviation for strain of a 1 cm-high sample was 2.78% (with a 95% confidence interval (+/- 2σ) of 2.64-2.92%). The standard deviation of a 2 cm-high sample was 1.33% (95% confidence interval of 1.24-1.42%). The Monte Carlo simulation properties and results are included in Table 6.6.

6.2 Compaction

The compaction dry density was calculated for samples of the main testing program. The target density was 1.55 g/cm^3 (maximum standard proctor) however the measured dry density varied from 1.47 to 1.63 g/cm^3 with a standard deviation of 0.04 g/cm^3. The average measured dry density was 1.553 g/cm^3. A histogram of compaction densities is included as Fig. 6.2 and the statistical measures are listed in Table 6.7.

The calculated standard deviation of 0.04 g/cm^3 was significantly larger than the expected standard deviation due to measurement error ($0.014 g/cm^3$). In order to determine how much scatter was a result of poor compaction the measured dry density was modeled as a normal distribution such that:

$$\gamma_{d,measured} = \gamma(1.55, \sigma_\gamma) + E_\gamma(0, 0.014) \tag{6.16}$$

The standard deviation of the dry density, σ_γ, corrected for measurement error was then calculated as:

$$\sigma_\gamma = \sqrt{\sigma^2_{\gamma_{d,measured}} - \sigma^2_{E_\gamma}} = 0.037 g/cc \tag{6.17}$$

The target dry density and +/- one corrected standard deviation is plotted against the standard proctor curve in Fig. 6.3. The resulting 67% confidence interval covers nearly the entire standard proctor density range and indicates poor compaction control. The possible sources of the poor compaction were from an incorrect mass of soil, sample height, or both.

The calculated masses of soil from eighteen tests with 2 cm-high samples are included in Table 6.8. The standard deviation of the data set was calculated as

Table 6.7: Compaction Dry Density of Samples (g/cm^3)

	1 cm Samples	2 cm Samples
Minimum	1.47	1.48
Maximum	1.63	1.61
Average	1.55	1.56
$\sigma_{\gamma_{d,measured}}$	0.04	0.04
$\sigma_{E_{\gamma_{d,measured}}}$	0.028	0.014
$\sigma_{\gamma_{d,corrected}}$	0.029	0.037

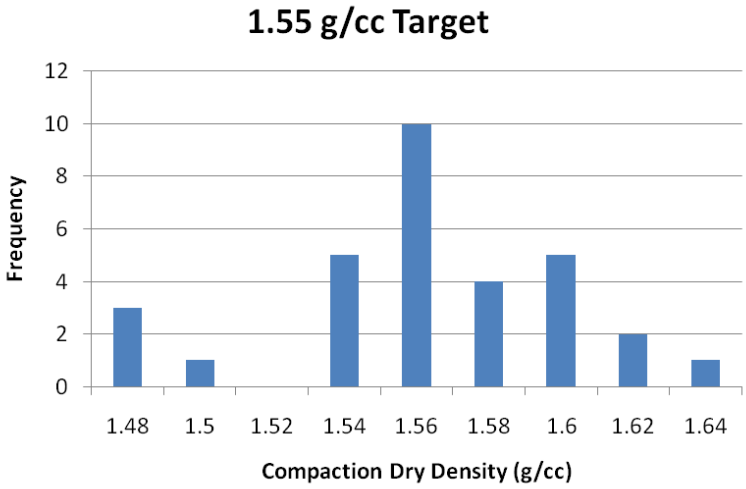

Figure 6.2: Measured Density of Samples

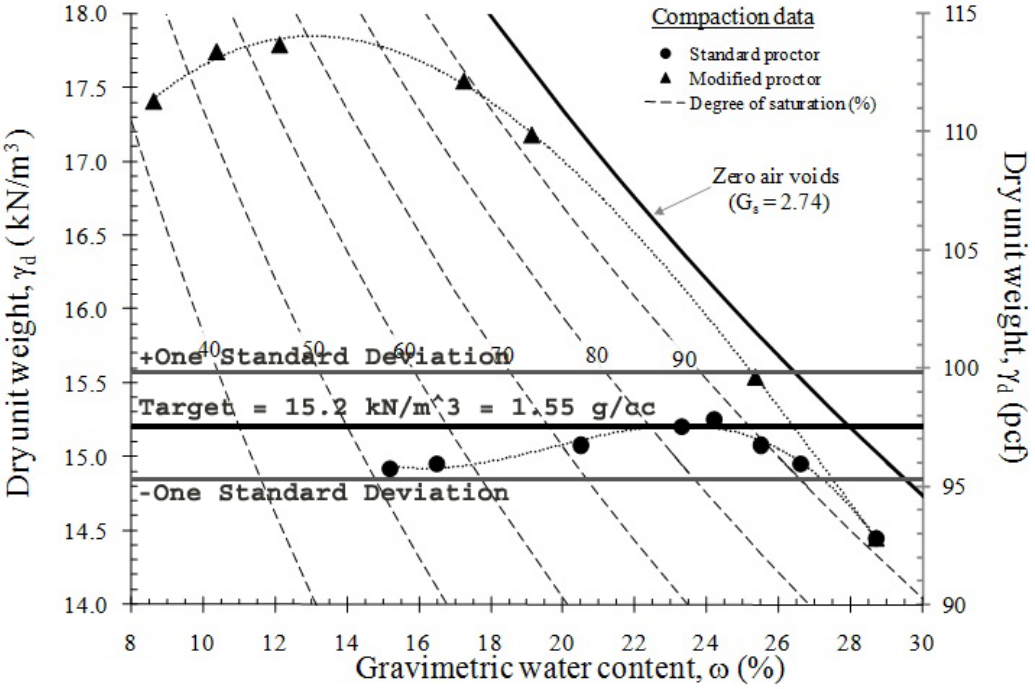

Figure 6.3: Compaction Scatter (2 cm samples)

Table 6.8: Calculated Mass of Soil (grams)

Soil Mass (g)				
98.55	98.54	98.56	98.46	99.16
99.24	99.27	99.16	98.28	99.28
97.52	98.79	98.56	98.46	98.15
98.36	98.62	98.68		
Average:			98.59	
Standard Deviation:			.44	

0.44 grams with an average of 98.59 grams. Using the same notation from Section 6.1.3.1 except modeling the mass of soil as a normal distribution instead of constant the calculated mass of soil was defined as:

$$M_{soil,calc} = M_{soil}(\mu_{M_{soil}}, \sigma_{M_{soil}}) + E_{M_{soil,calc}}(0, .01) \tag{6.18}$$

The standard deviation of the actual mass of soil was calculated using the standard deviation of the error and standard deviation of calculated soil mass using:

$$\sigma_{M_{soil}} = \sqrt{\sigma^2_{M_{soil,calc}} - \sigma^2_{E_{M_{soil,calc}}}} = 0.44g \approx \sigma_{M_{soil,calc}}$$

The standard deviation of the calculated soil mass is dominated by the standard deviation of soil mass and measurement error has no significant effect.

Similarly the calculated sample height was modeled as:

$$H_{ave,calc} = H_{ave}(\mu_{H_{ave}}, \sigma_{H_{ave}}) + E_{H_{ave,calc}}(0, 0.013) \tag{6.19}$$

where $H_{ave}()$ and $E_{H_{ave}}()$ were normal distributions of the sample height (average of two readings) and measurement error. Data of sample heights from tests were collected and grouped by target sample height. The averages and standard devia-

Table 6.9: Measured Sample Heights

1 cm Samples			2 cm Samples		
1.05	0.96	0.97	1.93	2.11	1.97
1.015	0.97	0.99	1.94	2.01	1.96
1.03	0.98	1.00	1.99	2.01	1.98
1.00	1.01	1.05	1.94	1.98	1.98
1.02	0.99	1.00	2.00	2.10	1.95
			1.97		
Average: 1.00 cm			Average: 1.99 cm		
Standard Deviation: 0.026 cm			Standard Deviation: 0.052 cm		
Corrected Standard Deviation: 0.023 cm			Corrected Standard Deviation: 0.050 cm		
Coefficient of Variance: 2.3%			Coefficient of Variance: 2.5%		

tions were then calculated and are included in Table 6.9. The standard deviations of sample height were corrected for measurement error as:

$$\sigma_{H_{ave}} = \sqrt{\sigma^2_{H_{ave,calc}} - \sigma^2_{E_{H_{ave,calc}}}} \tag{6.20}$$

The correction for measurement error was small and the majority of scatter seen in measured sample heights was not due to measurement error. The average height of the samples matched closely with the target for both 1 cm-high and 2 cm-high samples. The corrected standard deviation increased by over a factor of two from the 1 cm-high samples to the 2 cm-high samples. This suggested that the standard deviation was a function of sample height rather than an absolute distance. This was confirmed when the coefficient of variance was calculated for both and were nearly the same.

Histograms of measured sample heights for 1 cm-high and 2 cm-high samples were compiled, and are included as Fig. 6.4. The measured sample heights of 1 cm-high samples appear to be normally distributed. The 2 cm-high samples

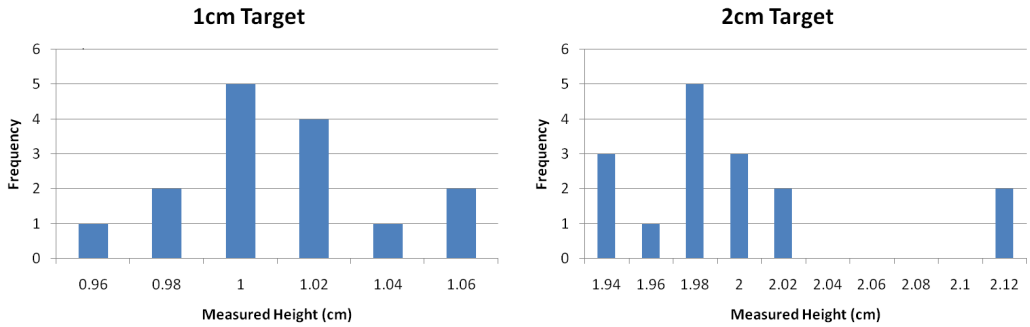

Figure 6.4: Measured Sample Heights

have a erratic distribution with samples generally over-compacted. Neither the data sets have enough points to make a definitive conclusion on their distributions however the distributions were close enough to normal that the assumption of a normal distribution used for calculation and correction of standard deviation was valid.

In order to determine whether the the source of the poor compaction was from incorrect sample heights or soil masses, correlation coefficients between sample height, soil mass, and dry density were calculated for both 1 cm-high and 2 cm-high samples. The resulting correlation coefficient matrix is included in Table 6.10. A strong correlation was found between sample height and dry density with a correlation coefficient of -0.88 and -0.99 for 1 cm-high and 2 cm-high samples respectively. Also of note was the positive correlation found between soil mass and sample height. The positive correlation meant that samples of higher mass tended to also be samples with a larger height resulting in a partial correction in dry density for samples with incorrect soil masses. There was little correlation found between soil mass and dry density. The correlation coefficient was 0.24 for 1 cm-high samples and -0.38 for 2 cm-high samples. Both data sets were combined

Table 6.10: Correlation Coefficients

	1 cm Samples			2 cm Samples		
	Sample Height	Soil Mass	Dry Density	Sample Height	Soil Mass	Dry Density
Sample Height	1	0.25	-0.88	1	0.52	-0.99
Soil Mass	0.25	1	0.24	0.52	1	-0.38
Dry Density	-0.88	0.24	1	-0.99	-0.38	1

by defining the sample height and soil mass as a percent error from the target such that:

$$\%Error = \frac{Actual - Target}{Target} \times 100 \tag{6.21}$$

The resulting correlation coefficient between dry density and soil mass was 0.06 indicating no correlation.

The error in sample height and soil mass were also plotted against dry density in Fig. 6.5 to illustrate the correlations. The soil mass (red squares) had no defined arrangement with dry density while the sample height (blue diamonds) had a tight arrangement.

The conclusion from the compaction analysis was that the control of sample height was the main cause for the range in dry density. Soil mass was generally lower than target but had no detectable impact on dry density. Attempts to improve compaction accuracy should focus on the control of sample height.

6.2.1 Effects of Compaction

The initial density of centrifuge samples varied significantly throughout the testing program. The range of sample heights and cause for poor compaction was

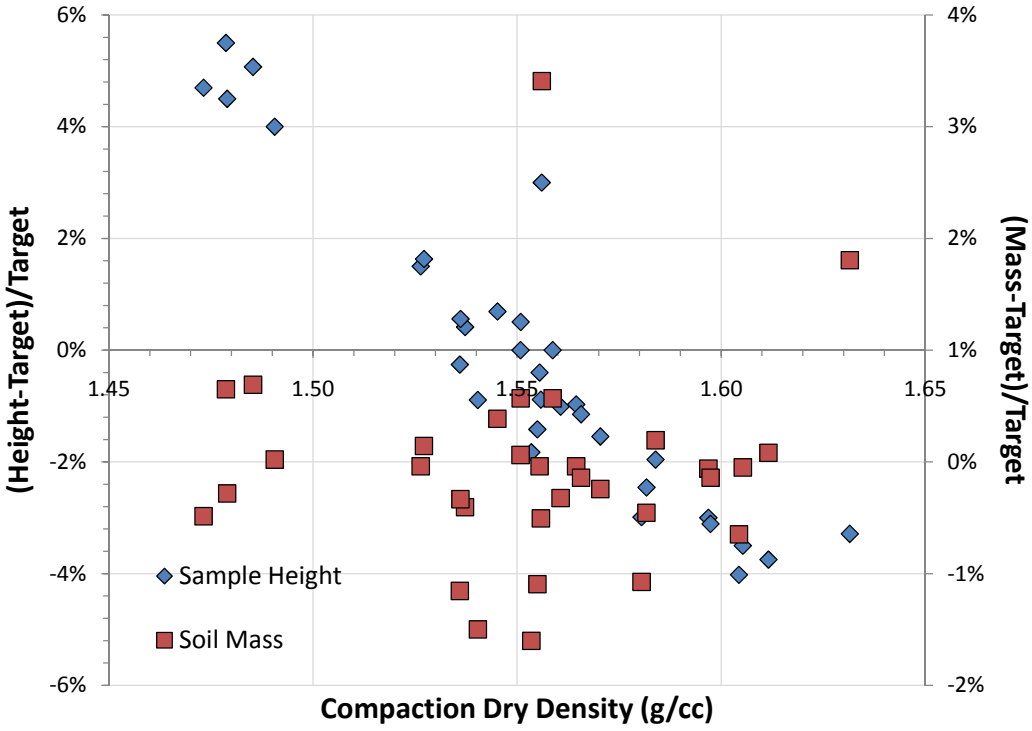

Figure 6.5: Dry Density Correlation (2 cm samples)

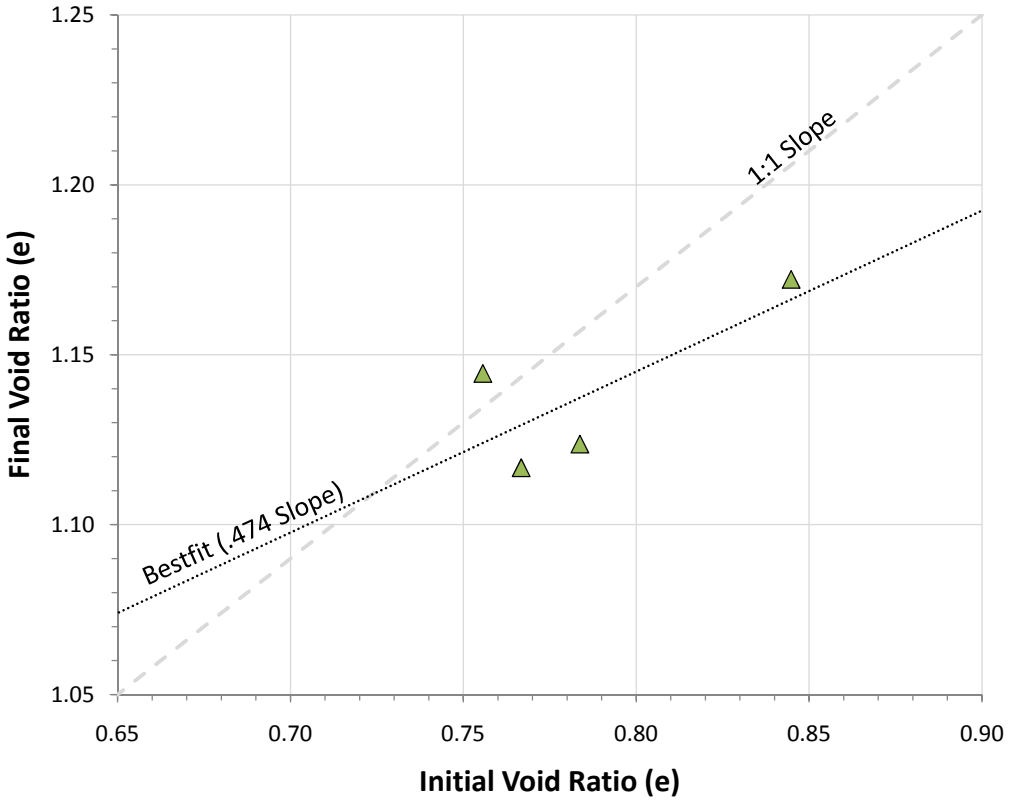

Figure 6.6: Void Ratio, 2 cm Samples - 30g

discussed in Section 6.2 however the effect the the compaction had on final properties such as total strain or void ratio was unknown. In order to determine the effect the compaction had, initial and final void ratio were calculated for three sets of tests. The test sets were composed of 2 cm-high samples flown at g-levels of 30, 105, and 350. The 30g and 350g test sets included four samples each while the 105g set included eight. The initial and final void ratio of samples in each test set can be seen in Figs. 6.6-6.8.

The sample sets of 30g and 105g tests had strong correlation between initial and final void ratio. Both sets of data showed increases in final void ratio with

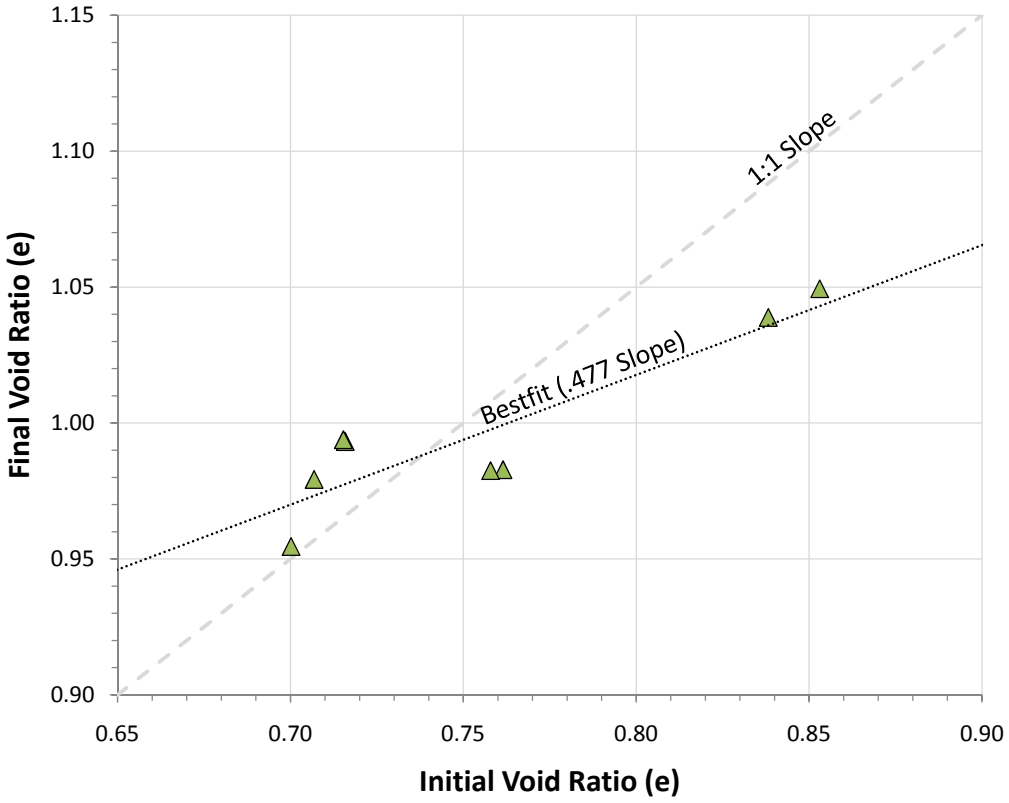

Figure 6.7: Void Ratio, 2 cm Samples - 105g

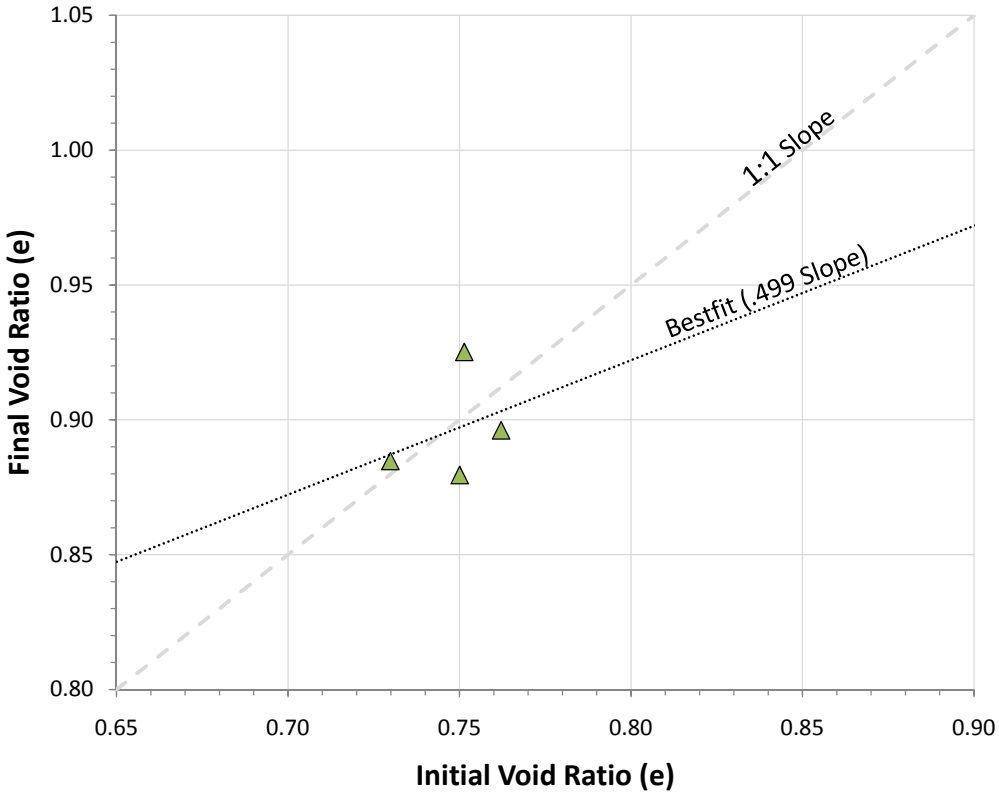

Figure 6.8: Void Ratio, 2 cm Samples - 350g

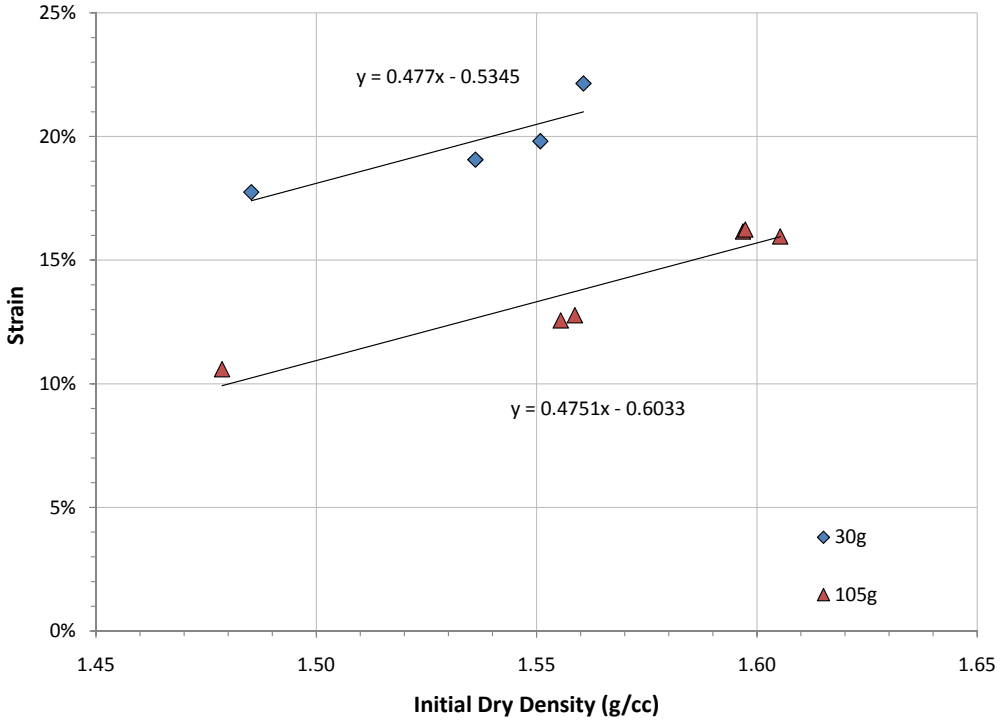

Figure 6.9: Effect of Compaction on Final Strain

increased initial void ratio. Linear best fit functions resulted in slopes of approximately 0.5 for both sets. The range in initial void ratio for the 350g data was too narrow to draw a meaningful relation between initial and final void ratio however the trend seen was similar to the 30g and 105g test sets. The relations calculated for initial dry density and final strain can be seen in Fig. 6.9.

A correction based on the relation between initial and final void ratio seen in the 30g and 105g test sets was then used to correct the measured final strain such that:

$$S\%_{corrected} = S\%_{measured} - 47.6(\rho_{d,measured} - \rho_{d,target}) \tag{6.22}$$

Table 6.11: Corrected Swell

Test ID	G level *	Water Head (cm)	Overburden (g)	Compaction Dry Density ($\frac{g}{cm^3}$)	Measured Swell (%)	Corrected Swell (%)
20	105*	2	12	1.61	16.0	13.3
21	105*	2	12	1.60	16.2	13.9
22	105*	2	12	1.56	12.6	12.3
23	105*	2	12	1.60	16.2	14.0
24	105*	2	12	1.56	12.8	12.4
25	105*	2	12	1.48	10.6	14.0
26	29	2	12	1.54	19.1	19.8
27	29	2	12	1.55	19.8	19.8
28	36	2	12	1.56	21.5	21.0
29	36	2	12	1.49	17.7	20.8
30	340	2	12	1.55	7.6	7.4
31	340	2	12	1.58	9	7.4
32	360	2	12	1.56	9.9	9.2
33	360	2	12	1.57	7.4	6.7
34	105*	2	40	1.58	12.9	11.4
35	105*	2	40	1.57	11.2	10.2

*Estimated from power level.

where density is measured in g/cm^3. The resulting corrected swells for the 2 cm-high testing program are included as Table 6.11. Correcting the swells resulted in significantly less scatter in final strain for each data set.

6.3 Stresses in Centrifuge Specimens

In order to perform analysis on the centrifuge results and relate them to 1g tests the effective stresses of the centrifuge samples were needed. In order to calculate the effective stresses, a framework for the analysis of stresses in the centrifuge was developed similar to the framework by Dell'Avanzi et al. [2004]. Flow in the new

framework is also calculated by gradient in fluid potential however fluid pressure was incorporated rather than suction as the samples were assumed saturated.

In order to calculate stresses in the centrifuge, the increased gravity experienced by samples in the centrifuges can be calculated as:

$$a_c = \omega^2 r = Ng \tag{6.23}$$

where a_c is the centripetal acceleration, ω is the rotational velocity, and r is the centrifuge radius. N denotes how many times the standard gravitational acceleration the sample experiences.

6.3.1 Soil Pressures

To determine the pressure caused by the soil the unit weight must be known. The unit weight however is dependent on the gravitational acceleration and is defined as:

$$\gamma = \rho a_g \tag{6.24}$$

The acceleration of centrifuge samples is dependent on gravity and Eqns. 6.23 and 6.24 were combined to determine the unit weight of a soil under centrifugal acceleration as:

$$\gamma_c = \rho \omega^2 r \tag{6.25}$$

Because the unit weight of a material is dependent on radius, the pressure caused by the soil must be calculated by integrating the unit weight over its radius:

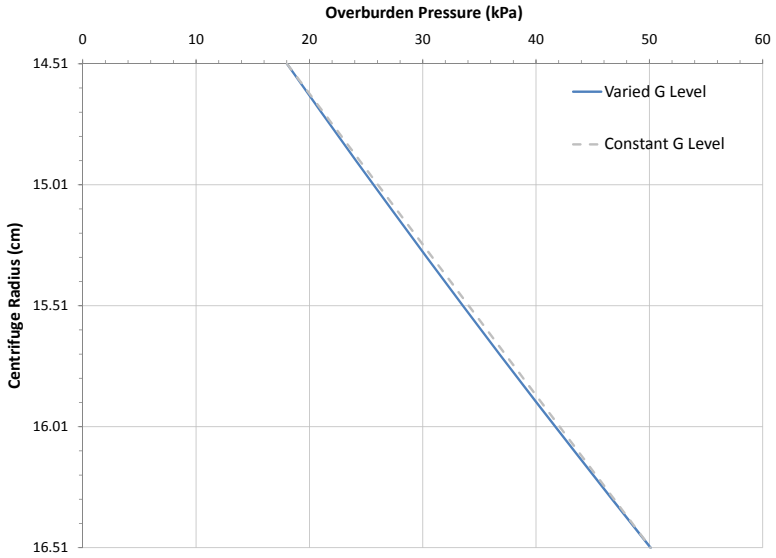

Figure 6.10: Total Soil Stresses

$$p(r) = p_t + \int_{r_t}^{r} \rho_s \omega^2 r dr = \frac{1}{2}\rho_s \omega^2 (r^2 - r_t^2) + p_t \tag{6.26}$$

where p_t and r_t are the pressure and radius of the top of the soil.

Soil pressures were calculated for a sample assuming a two centimeter sample height, two centimeter water head, and 780 RPM (approximately 100g at mid height of sample). The resulting pressures were graphed in Fig. 6.10. The top of the sample is at 14.51 cm while the base is at 16.51 cm. The blue line represents the calculated pressure across the sample considering an increasing g level with radius as seen in centrifuge testing. The dashed line represents the pressure expected in a constant g level (100g in this case) with the same initial pressure head. The pressures calculated for the centrifuge sample were slightly lower than those in constant g level due to the pressure in the centrifuge having a concave up parabolic distribution.

6.3.2 Pore Water Pressures

Pore water pressures in centrifuge samples were calculated by assuming steady state flow, saturation of samples, and Darcian flow. Given these assumptions the discharge velocity of centrifuge samples, v_c, was calculated as:

$$v_c = -\frac{k_s}{g}\frac{\delta \phi_c}{\delta r} \tag{6.27}$$

where g is the gravitational constant and $\frac{\delta \phi_c}{\delta r}$ is the gradient in fluid potential at radius r. Assuming the base of the sample, r_0, to be the elevation datum the fluid potential was as calculated as:

$$\phi_c = \frac{1}{2}\omega^2(r_0^2 - r^2) + \frac{P(r)}{\rho_w} \tag{6.28}$$

Taking the derivative of Equation 6.28 and substituting the result for $\frac{\delta \phi_c}{\delta r}$ in Equation 6.27 the discharge velocity became:

$$v_c = -\frac{k_s}{\rho_w g}\left(-\rho_w \omega^2 r + \frac{\delta P(r)}{\delta r}\right) \tag{6.29}$$

The discharge velocity is constant over radius and taking the derivative resulted in:

$$0 = \frac{k_s}{\rho_w g}\rho_w \omega^2 - \frac{k_s}{\rho_w g}\frac{\delta^2 P(r)}{\delta^2 r} \tag{6.30}$$

The second derivative of pressure was solved for resulting and then integrated twice resulting in pressure as a function of radius:

$$P(r) = \frac{1}{2}\rho_w \omega^2 r^2 + C_1 r + C_2 \tag{6.31}$$

The equation has two unknown constants that were solved for by imposing boundary conditions of pressure at the base and top of the sample such that:

$$P(r_0) = \frac{1}{2}\rho_w \omega^2 r_0^2 + C_1 r_0 + C_2 = 0 \tag{6.32}$$

$$P(r_t) = \frac{1}{2}\rho_w \omega^2 r_t^2 + C_1 r_t + C_2 = P_1 \tag{6.33}$$

where P_1 was the known water pressure at the top of the specimen. The resulting constants were:

$$P(r_0) = \frac{1}{2}\rho_w \omega^2 r_0^2 - \frac{1}{2}\rho_w \omega^2 r_0^2 = 0 \tag{6.34}$$

$$C_1 = \frac{-(C_2 + \frac{1}{2}\rho_w \omega^2 r_0^2)}{r_0} \tag{6.35}$$

$$C_2 = \frac{1}{2}\rho_w \omega^2 r_t r_0 + \frac{P_1 r_0}{r_0 - r_t} \tag{6.36}$$

The constants were substituted into Eqn. 6.31 and the resulting equation,

$$P(r) = \frac{1}{2}\rho_w \omega^2 r^2 - \frac{(\frac{1}{2}\rho_w \omega^2 r_t r_0 + \frac{P_1 r_0}{r_0 - r_t} + \frac{1}{2}\rho_w \omega^2 r_0^2)}{r_0} r + \frac{1}{2}\rho_w \omega^2 r_t r_0 + \frac{P_1 r_0}{r_0 - r_t} \; (r_t \leq r \leq r_0) \tag{6.37}$$

was used to calculate the pressure throughout centrifuge samples.

Pore pressures were calculated for a sample with the same properties as calculated for soil pressures. The pore pressures are a concave down parabolic distribution. The calculated pore pressures for a varied g level were slightly lower

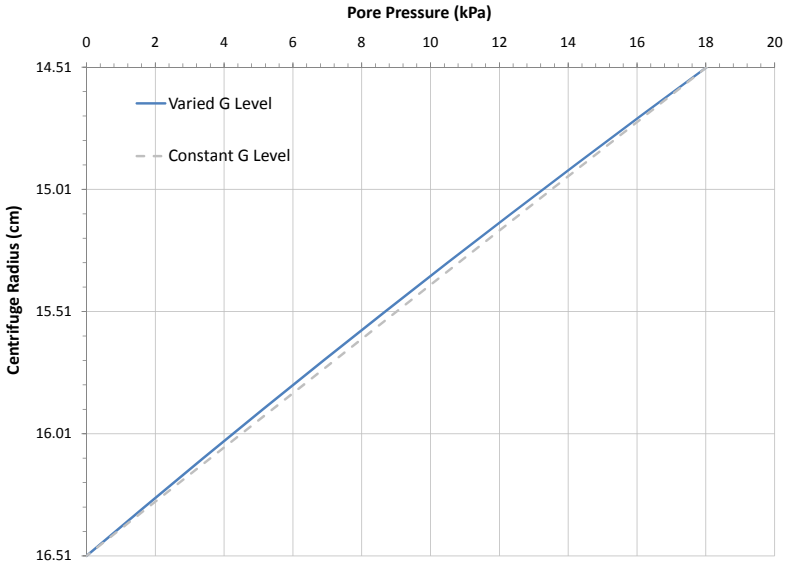

Figure 6.11: Pore Water Pressures

than those calculated for a constant g level with the maximum error at mid height.

6.3.3 Effective Stresses

Effective stress of samples in the centrifuge was calculated by subtracting the pore water pressure (Equation 6.37) from the total soil stress (Equation 6.26). The pressure, p_t, and pore pressure, P_1, at the top of the sample were calculated as:

$$p_t = \frac{1}{2}\rho_w\omega^2(r_t^2 - r_{tw}^2) + \sigma_{OB} \tag{6.38}$$

$$P_1 = \frac{1}{2}\rho_w\omega^2(r_t^2 - r_{tw}^2) \tag{6.39}$$

where r_{tw} was the radius at the water surface and σ_{OB} was the calculated overburden pressure on the top of the sample.

The resulting effective stresses, total stresses, and pore pressures were plot-

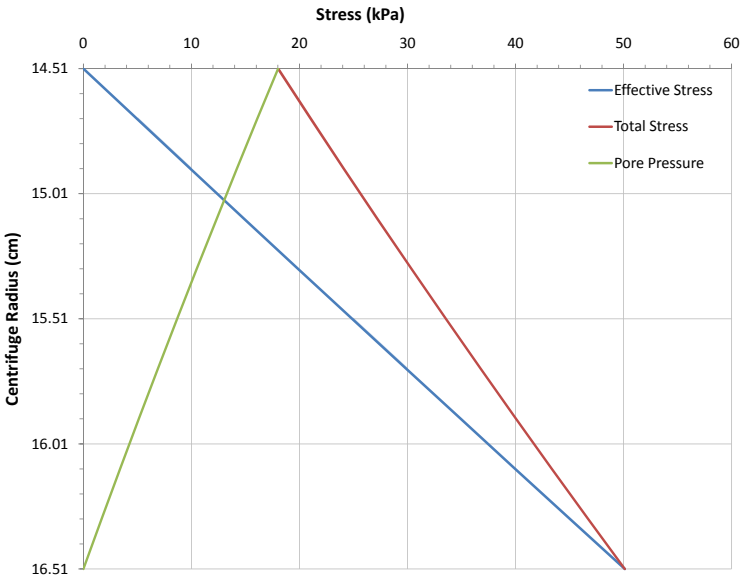

Figure 6.12: Stress Contours

ted in Fig. 6.12. The pressures were very similar to that of a constant g level environment. The effective stresses were so similar that they were indistinguishable on a plot and maximum errors were approximately 1%.

6.4 Determining Swelling Properties from Centrifuge Test Results

Two methods were developed for estimating the swell-stress relation from test results. Both were based on the assumption of a logarithmic relation between swelling strain and effective stress. The first method used two tests results and arithmetically solved for the two unknown coefficients of the assumed swell-stress relation. The second method used more than two test results and obtained a best fit logarithmic function (using Microsoft Excel's Solver). The methods are discussed

further in Sections 6.4.1 and 6.4.2.

Both methods required determination of the effective stress at the top ($\sigma_t^{'}$) and base ($\sigma_b^{'}$) of centrifuge tests as input. The stresses were calculated as:

$$\sigma_t^{'} = \frac{1}{2}\rho_w\omega^2(r_t^2 - r_{tw}^2) + \sigma_{OB} \tag{6.40}$$

$$\sigma_b^{'} = \frac{1}{2}\rho_w\omega^2(r_t^2 - r_{tw}^2) + \frac{1}{2}\rho_s\omega^2(r_b^2 - r_t^2) + \sigma_{OB} \tag{6.41}$$

where r_{tw}, r_t, r_b are the radii at the top of the water, top of the sample, and base of the sample respectively. The radii and density used were those of the final condition of the soil.

6.4.1 Arithmetic Method

The method was based on the assumption of a logarithmic swell-stress relation such that:

$$S\% = A\,ln(\sigma^{'}) + B \tag{6.42}$$

where $S\%$ is the percent swell expected, $\sigma^{'}$ is the effective stress, and A and B are unknown constants. A linear stress distribution was assumed across samples so that the expected swell of a sample could be calculated as the average of Eqn. 6.42 across the stress range experienced by the sample. The average was calculated as:

$$S\%_{ave} = \frac{\int_{\sigma_t^{'}}^{\sigma_b^{'}} S\%}{\sigma_b^{'} - \sigma_t^{'}} \tag{6.43}$$

where $\sigma_b^{'}$ and $\sigma_t^{'}$ are the effective stresses at the base and top of the sample. The integral of $S\%$ was calculated as:

$$\int S\% = A\,\sigma^{'}(ln(\sigma^{'}) + B') + C \tag{6.44}$$

where:

$$B' = -1 + B/A \tag{6.45}$$

A set of equations were formed such that:

$$S_1 = \frac{A\,\sigma_{b1}^{'}\left(ln(\sigma_{b1}^{'}) + B'\right) + C - A\,\sigma_{t1}^{'}\left(ln(\sigma_{t1}^{'}) + B'\right) - C}{\sigma_{b1}^{'} - \sigma_{t1}^{'}} \tag{6.46}$$

$$S_2 = \frac{A\,\sigma_{b2}^{'}\left(ln(\sigma_{b2}^{'}) + B'\right) + C - A\,\sigma_{t2}^{'}\left(ln(\sigma_{t2}^{'}) + B'\right) - C}{\sigma_{b2}^{'} - \sigma_{t2}^{'}} \tag{6.47}$$

where S_1 and S_2 were the measured total swell as percentages and $\sigma_{b1}^{'}$, $\sigma_{b2}^{'}$, $\sigma_{t1}^{'}$, and $\sigma_{t2}^{'}$ were the known effective stresses at the base and top of two tests. The unknowns A and B were then solved for such that:

$$A = \frac{(\sigma_{t1}^{'} - \sigma_{b1}^{'})S_1}{B(\sigma_{t1}^{'} - \sigma_{b1}^{'}) + \sigma_{t1}^{'}ln(\sigma_{t1}^{'}) - \sigma_{b1}^{'}ln(\sigma_{b1}^{'})} \tag{6.48}$$

and;

$$B' = \frac{S_1(\sigma_{t1}^{'} - \sigma_{b1}^{'})(\sigma_{b2}^{'}ln(\sigma_{b2}^{'}) - \sigma_{t2}^{'}ln(\sigma_{t2}^{'})) + S_2(\sigma_{b2}^{'} - \sigma_{b1}^{'})(\sigma_{b1}^{'}ln(\sigma_{b1}^{'}) - \sigma_{t1}^{'}ln(\sigma_{t1}^{'}))}{(\sigma_{t1}^{'} - \sigma_{b1}^{'})(S_2(\sigma_{b2}^{'} - \sigma_{t2}^{'}) + S_1(\sigma_{t2}^{'} - \sigma_{b2}^{'}))} \tag{6.49}$$

B' was then related back to B by:

$$B = B'A + A \tag{6.50}$$

The sensitivity of this analysis to errors in total measured swell was determined by calculating the swell-stress relation from the two tests listed under "Narrow Range" in Table 6.12. The swell-stress relation was first calculated with correct swell percentages, then assuming +1% error in swell on the first and second test, +1% error on the first test and -1% error on the second test, and finally -1% error on the first test and +1% error on the second. The resulting swell-stress relations are plotted in Fig. 6.13.

The errors in resulting swell-stress relation were minimized in the range of stresses used in the calibration. When the relation was extrapolated past the range in stresses seen in the two samples the errors were compounded. The swell-stress relations were recalculated for two samples with a much wider range in stresses ("Wide Range" in Table 6.12) and the errors had a much smaller effect on the overall relation.

The conclusion from the analysis was that if the swell-stress relation is determined using this method, the two calibration tests should be as far apart in range of stress as possible. The lower end should be tested at less than 25g and the upper end as high as possible (800g +). This would provide an accurate correlation between swell and stress for ranges in stress up to the swell pressure.

6.4.2 Best Fit Method

The second method evaluated for determining the swell-stress relation was for cases where more than two test results had been obtained. This method used the same formulation as the arithmetic method to calculate the total swell of a cen-

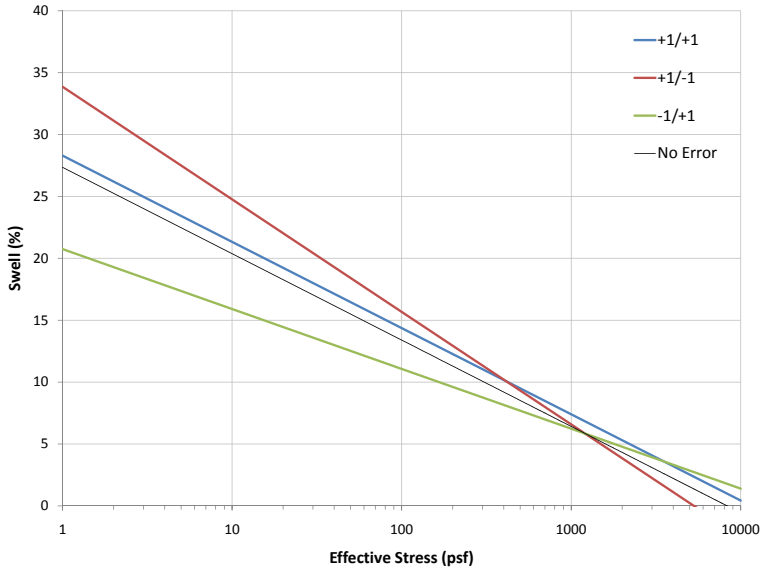

(a) Narrow Range

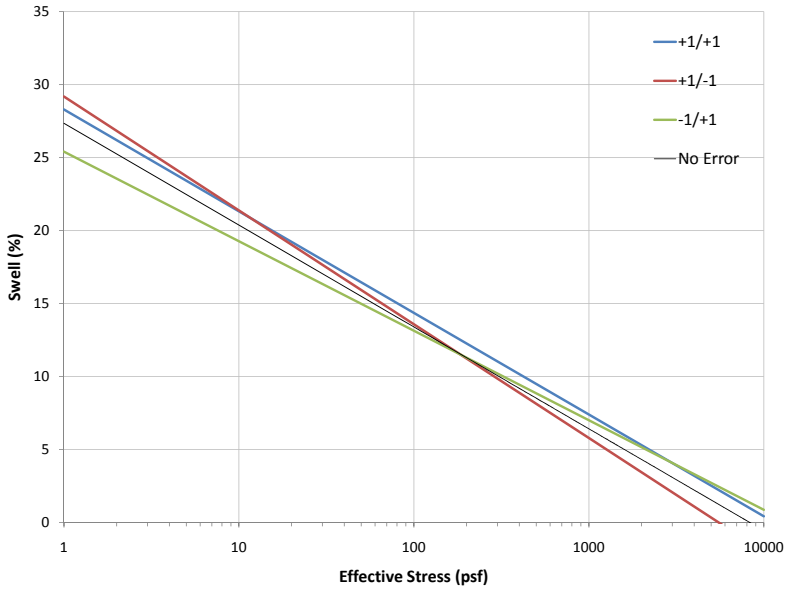

(b) Wide Range

Figure 6.13: Swell-Stress Errors (Arithmetic Method)

Table 6.12: Test Results For Calibration

Narrow Range			Wide Range		
	Test 1	Test 2		Test 1	Test 2
Strain (%)	9.1	2.6	Strain (%)	19.86	3.14
σ'_{top} (psf)	61.5	1280.4	σ'_{top} (psf)	5	2000
σ'_{base} (psf)	917.3	6521	σ'_{base} (psf)	20	4000

trifuge sample such that:

$$S\% = \frac{A\,\sigma'_b\left(ln(\sigma'_b) + B'\right) - A\,\sigma'_t\left(ln(\sigma'_t) + B'\right)}{\sigma'_b - \sigma'_t} \tag{6.51}$$

The method however, did not attempt to solve for the coefficients A and B' arithmetically and instead obtained them by the least squares method (using Solver from Microsoft Excel). Test data of the total measured swell and effective stresses at the top and base of samples were used in the calculations. Reasonable values were chosen for A and B' and swell was calculated for each test based on the effective stresses and the assumed swell-stress relation. The total error of the swell relation was calculated as:

$$Error = \sum_{i=1}^{n} \left(S_{measured,i} - S_{calculated,i}\right)^2 \tag{6.52}$$

The approach involved varying A and B' in order to minimize the calculated error. This method was in effect fitting a logarithmic function based on the least sum of squares. The method proved to be suitable for determining the swell-stress relation from multiple test results. The advantage of this method over the arithmetic version was that because additional tests were used, errors in each test had less effect on the overall swell-stress relation.

Table 6.13: Data for Arithmetic Method

Test ID	Initial Height (cm)	Final Height (cm)	Strain %	σ'_{top}(kPa)	σ'_{base} (kPa)
26	2.01	2.39	19.8	1.14	18.51
27	2.01	2.41	19.8	1.14	18.69
Average:			19.8	1.14	18.60
32	1.98	2.18	9.2	13.51	206.55
33	1.98	2.12	6.7	13.56	204.01
Average:			7.9	13.53	205.28

6.4.3 Results

Both methods discussed in Sections 6.4.1 and 6.4.2 were then used to predict the swell-stress relation using the testing results presented in Chapter 4. The arithmetic method was populated using the average strain from two 29g tests (Test ID 26 and 27) for the low end of stresses and the average of two 360g tests (Test ID 33 and 34) for the high end of stresses. The calculated effective stresses at the top and base of samples used for determining the swell-stress relation are included as Table 6.13. The resulting coefficients for the swell-stress relation are included in Table 6.15. The best fit method was populated with the entire two centimeter testing program. The calculated stresses are listed in Table 6.14 and the resulting coefficients for the swell-stress relation in Table 6.15.

The swell-stress relations calculated by both methods matched closely with one another. The error between the two was approximately 2% at 1 kPa and approximately 3% at 400 kPa (the approximate swell pressure). Plots of the resulting relations are included in Fig. 6.14.

The calculated swell-stress relation using the best fit method was then used to predict swell for the centrifuge test set using Eqn. 6.51. The error of the prediction was calculated as:

Table 6.14: Data for Arithmetic Method

Test ID	Initial Height (cm)	Final Height (cm)	Strain %	σ'_{top}(kPa)	σ'_{base} (kPa)
20	1.93	2.24	13.3	4.27	68.13
21	1.94	2.25	13.9	4.26	67.75
22	1.99	2.24	12.3	4.27	66.34
23	1.94	2.25	14.0	4.26	67.79
24	2.00	2.26	12.4	4.26	66.69
25	2.11	2.33	14.0	4.24	65.62
26	2.01	2.39	19.8	1.14	18.51
27	2.01	2.41	19.8	1.14	18.69
28	1.98	2.42	21.0	1.50	24.61
29	2.10	2.47	20.8	1.49	24.16
30	1.97	2.12	7.4	13.27	198.36
31	1.96	2.14	7.4	13.25	201.67
32	1.98	2.18	9.2	13.51	206.55
33	1.98	2.12	6.7	13.56	204.01
34	1.95	2.20	11.4	11.59	73.74
35	1.97	2.19	10.2	11.59	73.43

Table 6.15: Resulting Coefficients

Method	A	B
Arithmetic	-4.936	30.193
Best Fit	-5.607	32.470

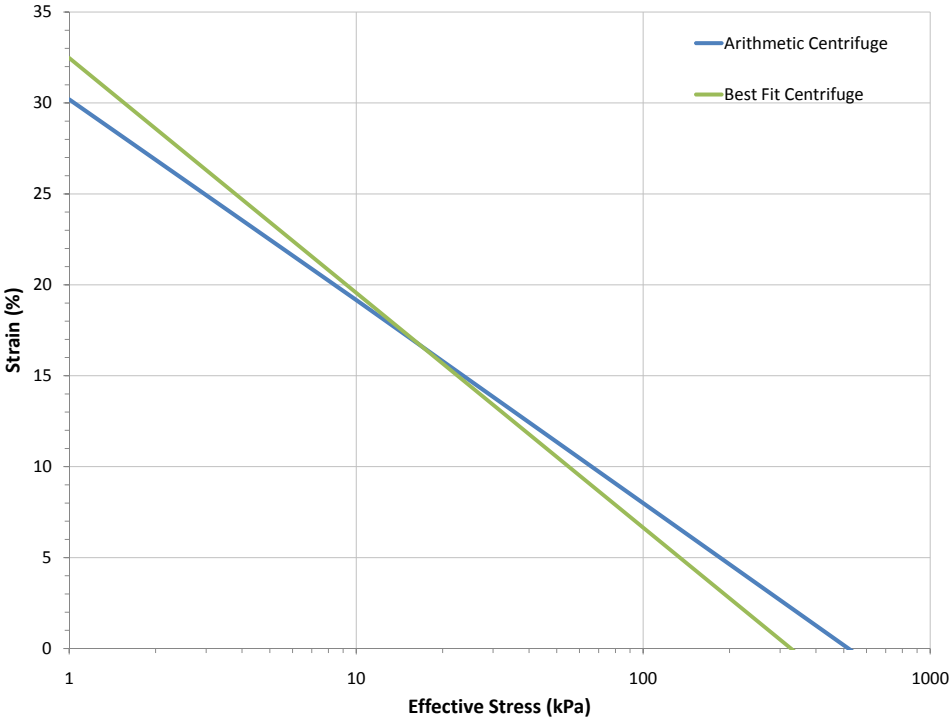

Figure 6.14: Swell-Stress Relations

Table 6.16: Accuracy of Swell Prediction

Test ID #	Error
20	-0.10
21	0.48
22	-1.20
23	0.53
24	-1.12
25	0.51
26	-0.91
27	-0.88
28	1.88
29	1.66
30	0.03
31	0.10
32	2.08
33	-0.54
34	-0.66
35	-1.84
Average:	0
Standard Deviation:	1.15

$$Error = Measured\ Swell\% - Predicted\ Swell\% \tag{6.53}$$

The resulting errors for of each test is included as Table 6.16. The standard deviation of the error was 1.15%. This standard deviation was similar to that expected due to measurement error of 1.33%.

6.5 Modeling of Centrifuge Samples

Centrifuge samples were modeled by breaking the samples into 20 discrete layers. Stresses were calculated at the interface of each layer using the equations derived in Section 6.3. Stress for each layer was taken as the average of the stresses calculated

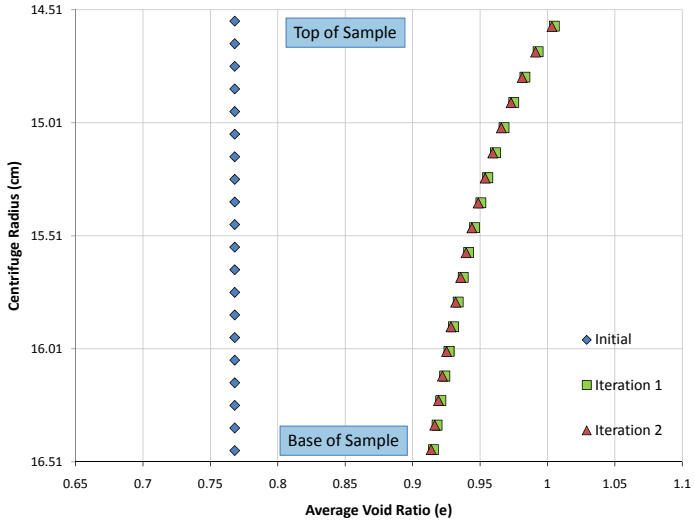

Figure 6.15: Average Layer Void Ratio

at the upper and lower interfaces. The swell of each layer was calculated from a given swell-stress relation. Void ratios were then corrected for the swell of the layer such that:

$$e_f = e_i \frac{S\%}{100} \tag{6.54}$$

where e_i and e_f were the void ratio before and after swell correction and $S\%$ was the calculated swell for the effective stress of the layer obtained from the swell-stress relationship. The density of soil of each layer was then updated based on the new void ratio assuming that the soil was saturated. Stresses throughout the sample were recalculated and this process was repeated until layer thicknesses converged. The final calculated sample height was found to be accurate within 0.01 cm after two iterations.

The void ratio calculated for each layer of a centrifuge sample was plotted

in Fig. 6.15. The plot includes the void ratios for the initial condition and after the first and second iterations. The difference in void ratio between the first and second iteration is minor with a slight decrease in void ratio from the first to second iteration.

The main problem with this modeling method was that the swell-stress relation must be known and input into the model in order to calculate the final sample height. This is effective for comparing centrifuge tests with a known swell-stress relation and validating the assumptions used. However in order for the centrifuge testing procedure to be useful it must be effective at producing the swell-stress relation rather than used to validate it. A method for determining the swell-stress relation from centrifuge tests is discussed in Section 6.4.

6.6 Water Contents

Water content data was collected throughout the testing program. Initially the water content of entire samples were taken together. In later testing samples were cut in half and water contents taken of both slices and in three tests the samples were cut into four slices and water contents taken for each slice.

The measured water contents for samples that were cut in two pieces is included in Table 6.18. The data set consists of four tests of approximately 30g, four of tests at approximately 350g, and two tests at 105g. The measured water contents were averaged for each g-level and graphed in Fig. 6.16. The water content of samples decreased with increasing stress as seen by lower water contents for the bottom slices and lower water contents for samples flown at higher g-level. The average degree of saturation of samples was 96%. A slight trend was found where samples at higher g-level tended to have a higher degree of saturation. The higher

Table 6.17: Measured Water Contents - Halves

G-Level	Water Content - Top (%)	Water Content - Base (%)	Degree of Saturation
105	36.2	31.6	96%
105	35.3	31.3	96%
360	34.9	30.5	96%
360	34.4	29.8	99%
340	33.5	29.2	96%
340	34.4	29.2	97%
36	42.2	36.8	92%
36	43.6	36.3	95%
29	43.0	35.6	96%
29	44.1	36.3	97%

degree of saturation may have been a result of the increased head and flow rate of high g-level samples.

The measured water contents of samples that were split into four pieces before measurement are included as Table 6.18. The water contents were plotted against approximate sample height to create the water content contours seen in Fig. 6.17. The three tests have similar water content contours however two of the tests show an increase in water content from the middle to the base of the sample. This was not expected as the base of the sample is the portion with the highest stresses.

One explanation is that when the samples were removed from the permeameter cup water from the outflow splashed onto the base of the sample. The additional water on the base of the sample could cause a larger than expected water content. This also is a problem on the top of the sample where water has been ponded. The top of samples were wiped with a dry paper towel before the water contents were taken in an attempt to remove excess moisture however it is a possibility that the measured water contents of the top and base were influenced by direct contact with water.

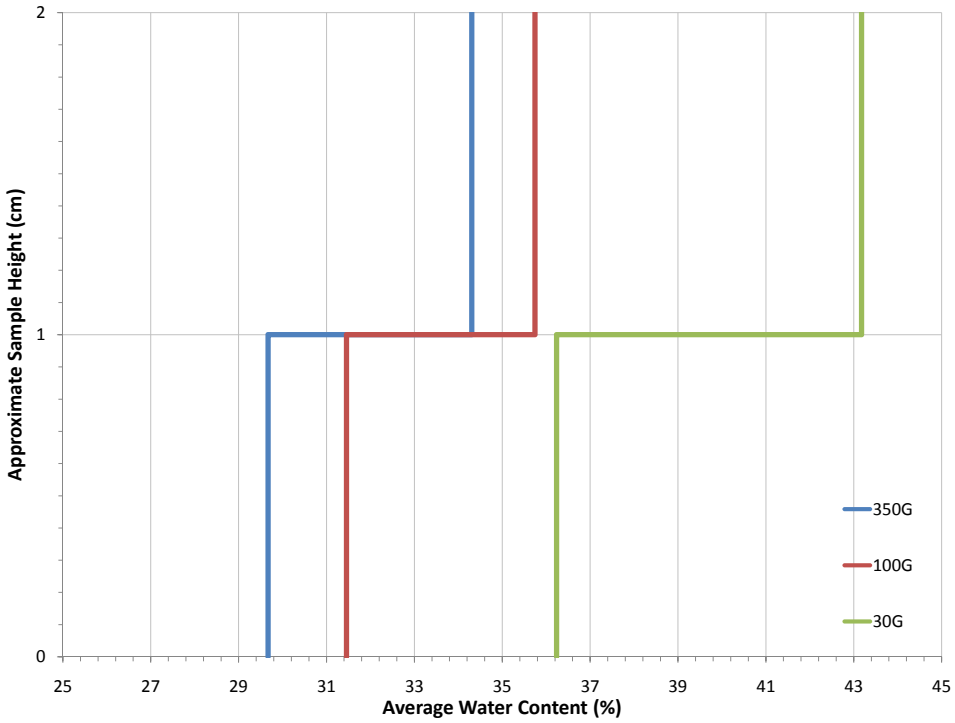

Figure 6.16: Measured Average Water Contents

Table 6.18: Measured Water Contents - Quarters

	Water Content (%)				Degree of
Final Height (cm)	Top	Upper Middle	Lower Middle	Base	Saturation
2.21	42.8	36.1	32.8	31.8	102%
2.31	43.3	34.3	33.6	35.5	95%
2.21	43.5	34.6	32.6	33.8	102%

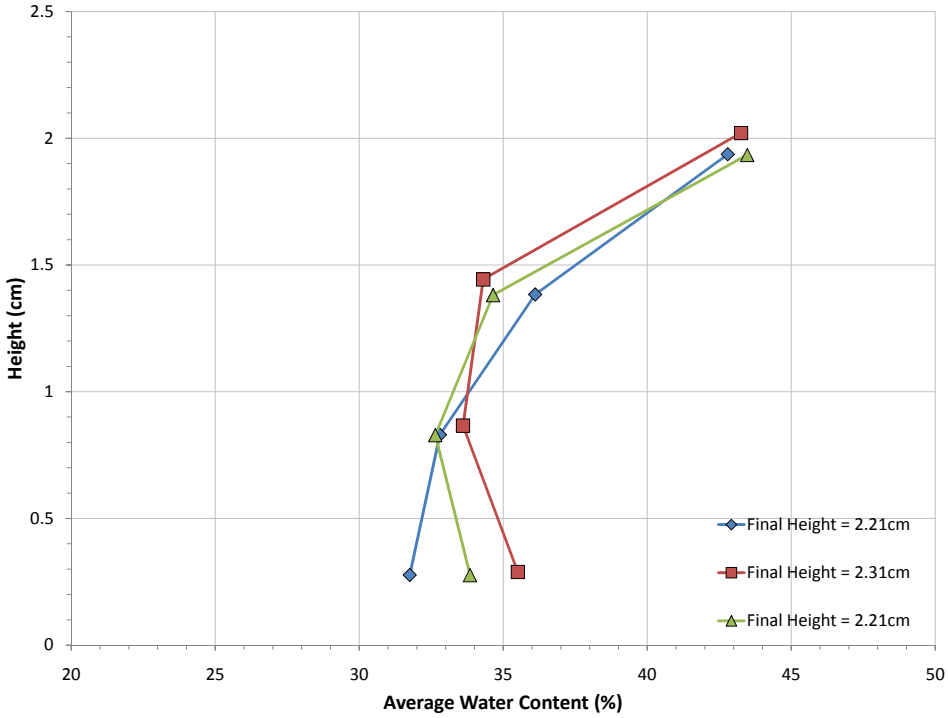

Figure 6.17: Water Content Contours

When samples were modeled using the procedure discussed in Section 6.5, the predicted water contents varied significantly from measured water contents. The predicted water contents assuming a 96% degree of saturation can be seen as the red line in Fig. 6.18. When compared to the measured water contents (blue line) the model predicts lower water contents at the surface and higher at the base. The measured contour seen in Fig. 6.18 was chosen as it did not have an increase in water content at the base likely due to direct contact with water from the outflow chamber.

The saturation of the modeled sample was then changed from being a constant 96% throughout the sample to a linear decreasing degree of saturation assuming 100% saturation at the top of the sample and 85% at the base. The resulting predicted water contents (green line) match more closely with the measured. The major differences are an under prediction of water content at the top and base of the sample. This could be explained by the over measurement of water content due to excess moisture on the surface of samples.

Overall the measured water contents in the centrifuge matched well with the modeled water contents. Several things were assumed such as the degree of saturation throughout the sample. This could be measured for each slice if the height of each slice was accurately measured. Unfortunately in the tests listed above samples were cut into approximate slices with no attempt to exactly measure the heights. The effect of extra water on the top and base of samples was also not known. If thinner slices were taken the theory of over measurement of water content due to direct contact with water on the sample could be validated.

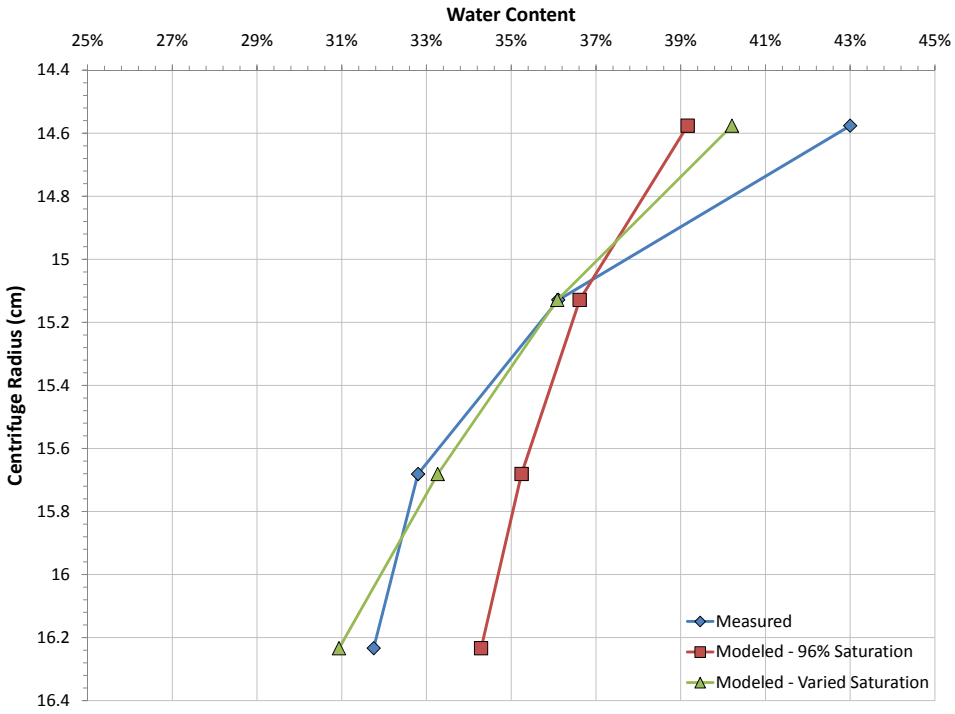

Figure 6.18: Measured vs. Modeled Water Contents

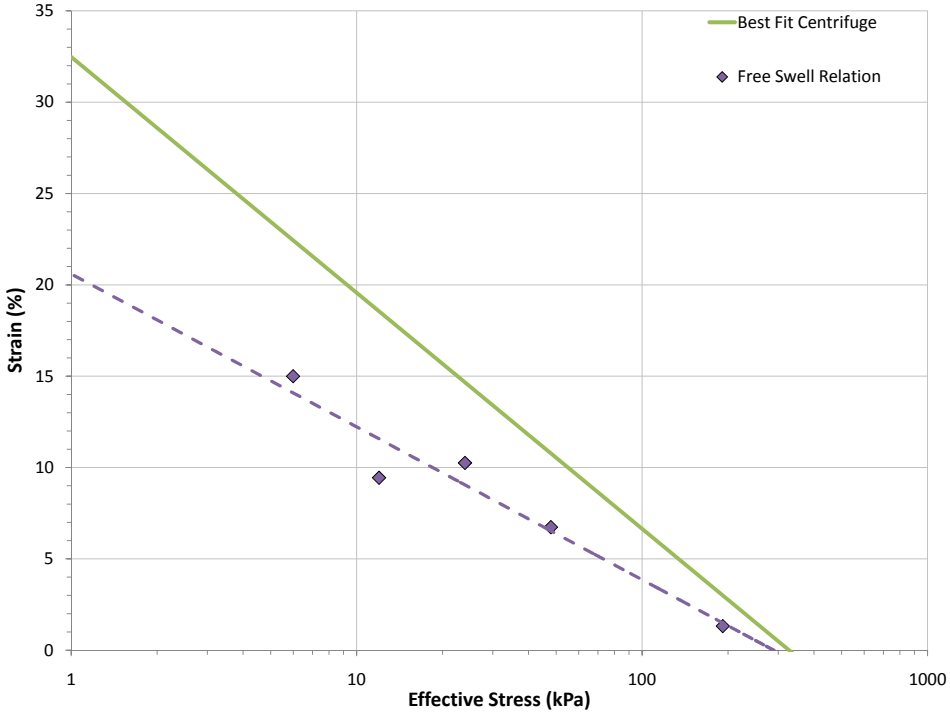

Figure 6.19: Centrifuge and Free Swell Relations

6.7 Comparison of results from Centrifuge and Free Swell Tests

The swell-stress relation determined using the best fit method was used for comparison with free swell tests as this relation was populated with all of the centrifuge test data. A graph of both the centrifuge relationship and the free swell relationship is included in Fig. 6.19. The swell-stress relationship found from the centrifuge tests did not match well with the relationship obtained from standard free swell tests. The percent error and magnitude error between the relationships at each stress level were calculated as:

$$Percent\ Error = \frac{S\%(\sigma')_{cent} - S\%(\sigma')_{freeswell}}{S\%_{freeswell}} \tag{6.55}$$

$$Error\ Magnitude = S\%(\sigma')_{cent} - S\%(\sigma')_{freeswell} \tag{6.56}$$

Graphs of the resulting errors as a function of effective stress are plotted as Fig. 6.20. The centrifuge relationship predicted significantly more swell than the free swell relationship. The magnitude of over-prediction ranged from nearly 10% at 1kPa to 2% at the swell pressure (determined by free swell tests). The percent error ranged from approximately 50% at 1kPa and increased as the predicted swell by free swell tests decreased.

In order to determine the effect the error between the relations would have on field applications, an example illustrating the total swell for a soil profile was calculated. Two soil profiles were analyzed. Both profiles were assumed to have an overburden of 1kPa representative of a base course or residential foundation. The depth of soil of the first profile was five meters to be representative of a typical active zone (Section 2.1.2). The second profile had used depths that would result in an effective stress at the base of the profile equal to the swell pressure of each relation. The swell pressure occured at a depth of 29.6 meters for the free swell relation and 53.6 meters for the relation from centrifuge best fit. The profile to the depth of swell pressure was chosen as the upper boundary of predicted swell.

The stresses for both profiles were calculated assuming a saturated density of 2 g/cm^3 and a water table at or above the soil surface. The predicted swells are representative of a soil profile that was compacted to maximum standard proctor density and then became saturated. The resulting swell predictions for the two soil

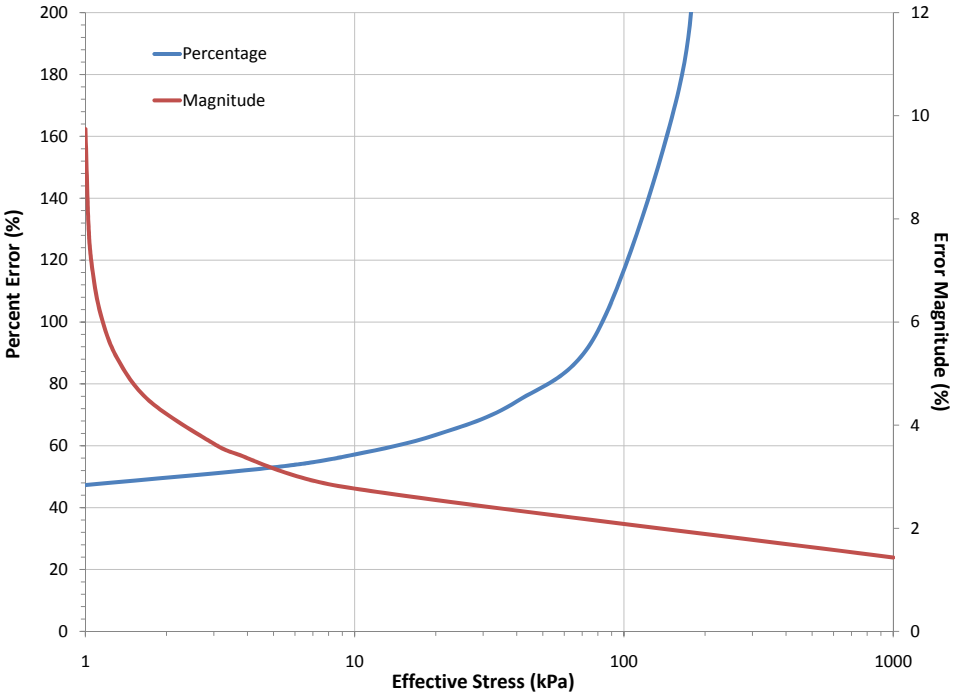

Figure 6.20: Centrifuge Prediction Error

Table 6.19: Swell Errors

	Soil Profile Depth	
	Active Zone	Swell Pressure
Centrifuge Predicted Swell (%)	15.9	4.7
Free Swell Predicted Swell (%)	7.8	3.5
Percent Error	63	36
Error Magnitude (%)	6.17	1.26
Centrifuge Predicted Swell (m)	0.80	2.54
Free Swell Predicted Swell (m)	0.49	1.03
Percent Error	63	146
Error Magnitude (m)	0.31	1.51

profiles are included as Table 6.19.

The resulting errors between the predictions were extremely high. The centrifuge relation predicted swell of the soil surface as 63% higher than the free swell relation for the active zone profile and 146% higher for the swell pressure profile. The magnitude of errors were 0.31m and 1.51m respectively. The error of 63% for the active zone profile was a better indication of the expected error if the centrifuge relation was used. The higher error of 146% from the swell pressure profile was mostly due to the larger depth of soil used in calculation for the centrifuge relation rather than the error in swell relation. The larger depth calculated to the swell pressure would not be an issue as moisture variations would not penetrate as deep as either swell pressure. The calculated error of 63% for the active zone profile was still too large to allow the swell-stress relation from the centrifuge tests to be useful for field applications.

The cause for the difference between swell-stress relations of the centrifuge and free swell tests was then explored. The effect of compaction, error due to height measurement procedure, and different stress paths were all examined and are discussed in Sections 6.7.1 and 6.7.2.

6.7.1 Height Measurement

Different procedures for the measurement of sample height had been adopted in centrifuge tests and the free swell tests. The sample height of the centrifuge tests was measured according to the procedure discussed in Section 4.2.4, which involved the ponding of water on top of samples. This procedure was developed to accurately measure the average height of compacted specimens with irregular surfaces. The sample heights of free swell tests were measured by dial indicators attached to the consolidation frames used in testing. The dial indicators measured the displacement of loading caps on the surface of samples.

When a sample with a flat surface is considered the two procedures are expected to result in the same measured height (assuming both are calibrated correctly). However the methods would result in different measured heights for samples with uneven surfaces. An irregular sample surface is illustrated in Figure 6.21. The loading cap (gray) rests on the peaks of the surface of the soil sample. When the sample height is measured from the loading cap, the height after correcting for the loading cap height is representative of the tallest portions of the sample. The testing procedure for centrifuge tests measures to the surface of a fluid (water) rather than rigid surface and the fluid molds to the shape of irregular sample surface. The difference in volume measured between the two procedures is shaded red in Fig. 6.21.

This difference in volume would occur during the initial measurements of height where the sample surface was uneven. Once the sample was exposed to water it would expand up to the loading cap creating an even surface. Until this point, the dial indicators in the free swell tests would have measured no displacement while the centrifuge testing procedure would have measured an increase in

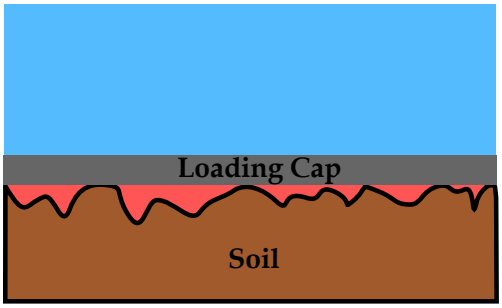

Figure 6.21: Height Measurement Error

height. The result is an increased measured swell using the measurement procedure adopted in the centrifuge and could explain some of the difference between the swell-stress relations found from centrifuge and free swell tests.

In an attempt to quantify the difference between the two procedures a centrifuge test was run using a new method for height measurement similar to the free swell procedure in addition to the standard centrifuge test procedure. The new measurement procedure measured the height of the sample using the mounted caliper shown in Figure 6.22. The height was measured from the top of the porous plate on top of the sample.

The testing results verified the assumption that the centrifuge testing procedure results in higher measured strains. Figure 6.22 includes the measured initial and final height using both procedures. The strain measured over time is included in Fig. 6.23a. It was not possible to conclude an accurate magnitude of error between the two methods based on the single test due to the scatter from the centrifuge testing results. For this single test the difference in strain was approximately 2% based on best fit lines for both procedures. However this difference could be solely from an error in initial height reading and more tests would be required to make definitive conclusions.

Figure 6.22: Mounted Caliper

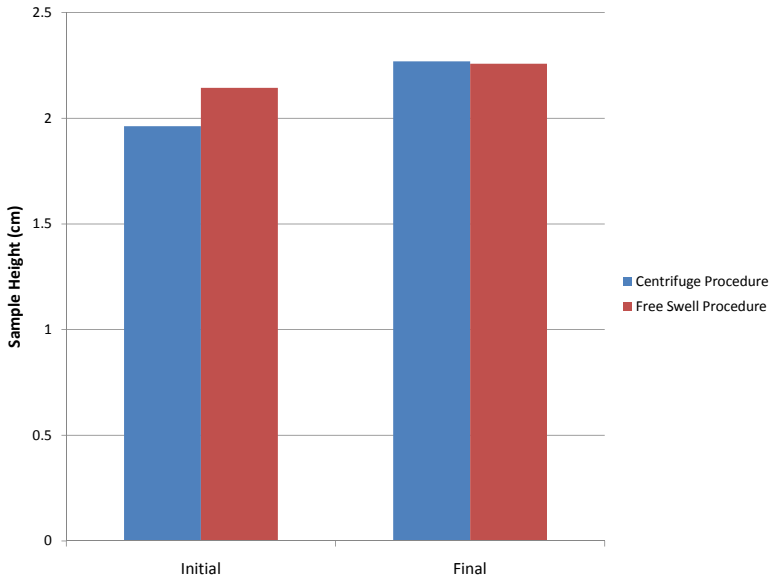

(a) Sample Heights

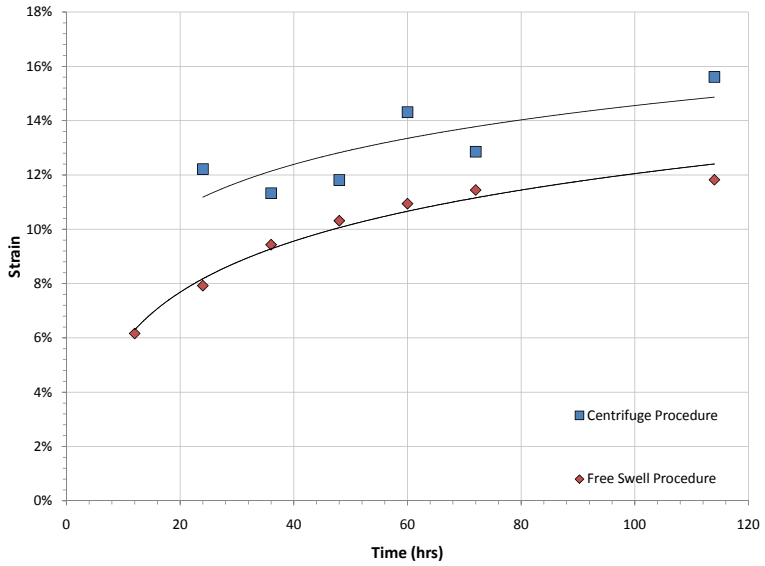

(b) Strains

Figure 6.23: Testing Procedure Comparison

6.7.2 Stress Path

One of the possible causes for the difference in predicted swell-stress relations was the time at which sample heights were measured. The initial heights were measured before the samples were under the increased stress due to centrifugation. The final heights were measured after the samples were removed from the increased stress. Figure 6.24 illustrates possible height changes in a centrifuge sample throughout testing. Point 1 is the initial height measurement before the sample is placed into the centrifuge. Once in the centrifuge, the increased stress experienced causes some compression of the sample. The height after the initial compression is shown as point 2. The sample then swells until reaching an equilibrium state in the centrifuge (Point 3). Once removed the sample expands due to reduced stress throughout the sample and the final measured height is shown as point 4. The same stress path occurs in the free swell tests however the points taken for strain measurement are different. The initial height is taken after the initial consolidation and compression of the sample (Point 2) and the final is taken before the expansion (Point 3).

In order to determine the effect the time of measurement had on the centrifuge and free swell tests had, two additional free swell tests were performed. The two tests were compacted exactly to one centimeter and consolidated under pressures of 12kPa and 96kPa (250 and 2000 psf). The initial compression was measured however it was difficult to accurately determine the settlement due to large deflections while the loading cap was seated. From the initial test set and the additional two test a relation for the compression of a 1 cm-high sample was estimated as:

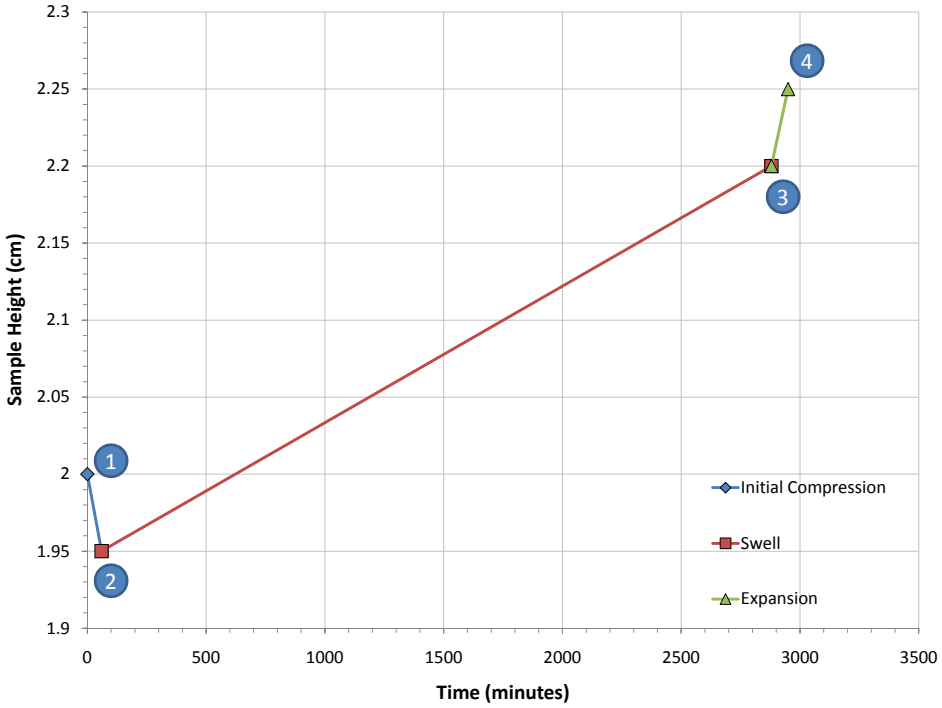

Figure 6.24: Stress Path

Table 6.20: Free Swell Tests

Stress (kPa)	Initial Height (cm)	Initial Compression (cm)	Swell (cm)	Final Expansion (cm)	Final Height (cm)
12	1.00	0.002	0.063	0.010	1.176
96	1.00	0.051	0.008	0.014	1.113

$$Compression\ (cm) = 0.0237 ln\sigma^{'} - 0.0569 \tag{6.57}$$

where the effective stress was measured in kPa. Swell was measured for 48 hours by LVDT and dial indicator. The water around the sample was then suctioned off and the overburden pressure reduced to zero and the expansion due to reduce stress was measured. The samples were then removed and final heights measured using a mounted caliper. The measured heights and deflections are included in Table 6.20.

When the test results were examined, a large discrepancy was noticed between the measured final height and the final height calculated based on initial height and deflections. The final height of a sample should equal the initial height minus the compression plus the swell and expansion. However the predicted final heights were 0.1 cm lower than the final measured heights, an error of 10%. The predicted and measured heights can be seen in Table 6.21.

There were only two times in which the samples could have swelled beyond that measured by dial indicator. These were between the initial height measurement and the sample being put in the consolidation frame and between the sample being taken out and the final height measured. In order to determine if either of these could account for approximately 0.1 cm of swell two samples were compacted to a height of one centimeter and then left in the cell for approximately

Table 6.21: Measured and Predicted Final Height

Stress (kPa)	Initial Height (cm)	Measured Final Height (cm)	Predicted Height (cm)	Error (cm)
12	1.00	1.18	1.07	0.10
96	1.00	1.11	0.97	0.14

15 minutes. The samples were subjected t omovements typical of what samples might experience when being loaded into a consolidation frame. The heights were then remeasured and and compared with the initial. The heights were found to increase 0.01 and 0.03 centimeters.

The increase in height between measurements could be explained by the samples rebounding. During compaction some stresses were trapped in the samples and resisted by ring friction and the samples expanded as these stresses were relieved. However the magnitude of change was small compared to the error found between predicted and measured final heights. This meant that a large portion of the error came after the sample was removed from the consolidation swell and measured. Additional free swell testing to verify the swell after removal was not completed because of time constraints.

The findings suggest that the free swell data collected in the main testing program (under 1g), while consistent with testing practice, was likely inaccurate. While deflections measured were correct, they did not account for additional swell when the sample was out of the consolidation frame. Ideally the height after the initial compression and consolidation (Point 2, Fig. 6.24) would be used as the initial height and the height after swell (Point 3, Fig. 6.24) would be the final. If additional swell tests were performed the rebound of the compaction sample could be measured and the initial and final heights calculated accurately. The strains

calculated using the correct heights would still differ from the centrifuge test results where the initial (Point 1, Fig. 6.24) and final (Point 4, Fig. 6.24) heights were taken when the sample was in a natural gravitational field and under low stresses.

The two additional swell tests do give some additional insight into the swell-strain behavior measured in the centrifuge. When the strain was calculated for the free swell tests from the initial and final measured heights (Points 1 and 4, Fig. 6.24) the swells matched reasonably well with the swell-stress relation calculated from centrifuge tests. The swell of the two additional free swell tests calculated from the measured initial and final heights was plotted against the centrifuge swell-stress relation in Fig. 6.25. The 12kPa test was approximately 1% below the the centrifuge relation while the swell for the 96kPa test was approximately 3% higher than the prediction by the centrifuge relation.

6.7.3 Summary

The swell-stress relations found using the centrifuge testing procedure and free swell testing matched well with each other. However, such match could only be defined after differences in testing procedures were accounted for and was based on only two free swell tests. The major difference between the two testing procedures and the cause for the difference in results was due to the time at which sample heights were measured.

As the centrifuge did not have in flight data acquisition the sample heights were measured before the samples were placed in the increased g-level environment and after they were taken out. This was different from the standard free swell tests where the swell was measured while the overburden pressure was still applied. When the free swell tests were measured in a manner similar to the cen-

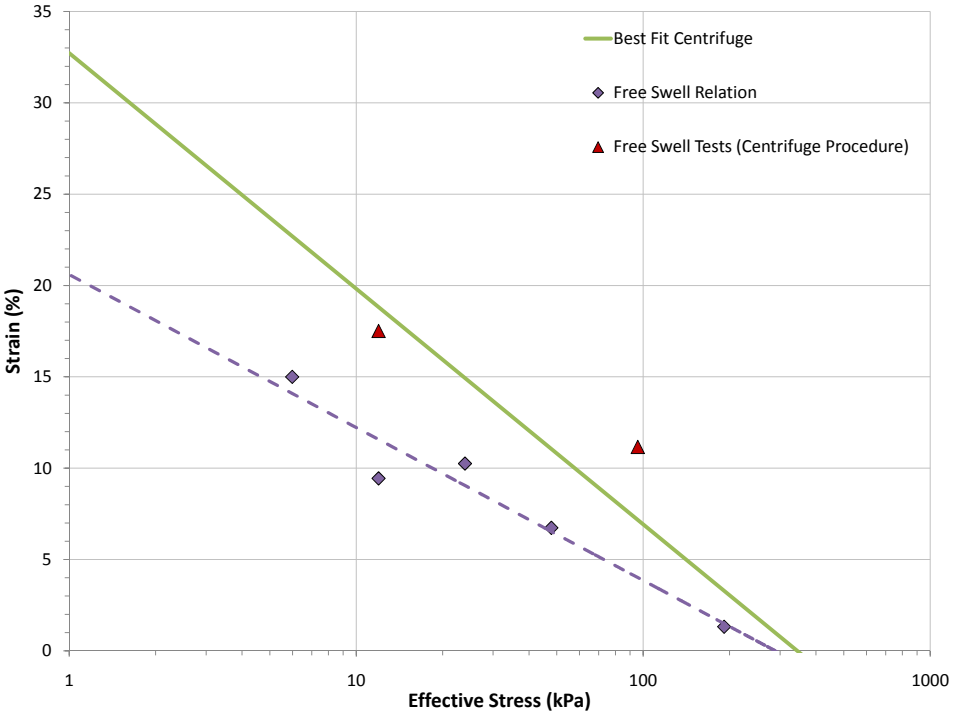

Figure 6.25: Additional Free Swell Points

trifuge tests (before being placed in the consolidation cell and after being taken out) the resulting swells matched reasonably well with the swell-stress relation found in the centrifuge.

This suggests that the method for calculation of stresses in the centrifuge and method for determining the swell-stress relation from centrifuge tests was accurate. If data acquisition was added to the centrifuge and the initial and final heights of centrifuge samples were taken while under the increased stress from centrifugation, the resulting swell-stress relation should be the same as one calculated using free swell tests. Additional free swell tests using the centrifuge testing procedure should be performed in order to further validate the comparison.

Chapter 7

Conclusions

Tests were performed on compacted specimens of Eagle Ford clay to evaluate the swelling potential of expansive clays using centrifuge testing. The main conclusions obtained after analysis of both centrifuge and free swell test results are:

- A testing procedure was developed for the testing of expansive soils in small centrifuges without data acquisition.
- Errors in height measurement resulted in one centimeter samples having a large scatter in test results. The height measurement error did not scale with sample height resulting in more consistent results for two centimeter samples.
- Compaction density had a substantial effect on the final swell of samples. Samples compacted below target density resulted in higher strains and lower final void ratios. Samples compacted above target density resulted in lower strains and higher final void ratios. A correction for final strain was derived for errors in compaction density. Once applied the final strain of samples in duplicate tests was consistent.

- A framework was developed for analyzing stresses in centrifuge samples accounting for variable g-level across samples. This framework allowed the entire swell-stress relation of a soil to be calculated arithmetically using two centrifuge test results. A method was also suggested for determining the swell-stress relation from data including more than two test results. Both methods resulted in a consistent prediction of the swell-stress relation. The arithmetic method was more sensitive to errors in input data however was accurate within the ranges of stress that populated the data.

- The swell-stress relationship found using centrifuge tests matched with the relationship found from free swell tests when the free swell tests were performed with a procedure similar to the centrifuge test procedure. The major difference between the two procedures was that the centrifuge samples were removed from the increased gravitational field of the centrifuge before reading were taken.

Bibliography

ASTMD-4546-08. Standard test methods for one-dimensional swell or collapse of cohesive soils. *American Society for Testing and Materials*.

A. Basma, A. Al-Homoud, A. Husein Malkawi, and M. Al-Bashabsheh. Swelling-shrinkage behavior of natural expansive clays. *Applied Clay Science*, 11(2-4):211–227, 1996. ISSN 01691317.

M. C. Caputo and J. R. Nimmo. Quasi-steady centrifuge method for unsaturated hydraulic properties. *WATER RESOURCES RESEARCH*, 41:5, 2005.

K. W. Cargill and H. Y. Ko. Centrifugal modelling of transient water flow. *Journal of Geotechnical Engineering*, 109(4):536–555, 1983. ISSN 07339410.

O. Cinicioglu, D. Znidarcic, and H.-Y. Ko. A new centrifugal testing method: Descending gravity test. *Geotechnical Testing Journal*, 29(5):355–364, 2006. ISSN 01496115.

E. Dell'Avanzi, J. Zornberg, and A. Cabral. uction profiles and scale factors for unsaturated flow under increased gravitational field. *Soils and Foundations*, 44 (3): 79–89, 2004.

V. Ferber, J.-C. Auriol, Y.-J. Cui, and J.-P. Magnan. On the swelling potential of

compacted high plasticity clays. *Engineering Geology*, 104(3-4):200–210, 2009. ISSN 00137952.

S. Frydman and E. Weisberg. Study of centrifuge modeling of swelling clay. *Proceedings of the International Conference Centrifuge 1991*, 0:113–113, 1991.

A. D. Gadre and V. S. Chandrasekaran. Swelling of black cotton soil using centrifuge modeling. *Journal of Geotechnical Engineering*, 120 (5):914–919, 1994.

D. Goodings. Relationships for modelling water effects in geotechnical centrifuge models. In *Proceedings of a Symposium on the Application of Centrifuge Modelling to Geotechnical Design.*, pages 1–24, Manchester, Engl, 1985. A. A. Balkema.

E. D. Hanafy. Swelling/shrinkage characteristic curve of desiccated expansive clays. *Geotechnical Testing Journal*, 14(2):206–211, 1991. ISSN 01496115.

D. E. Jones and W. G. Holtz. Expansive soils - the hidden disaster. *Civil Engineering*, 43.8:49–51, 1973.

D. T. Kennedy and R. J. Mitchell. Centrifuge modelling of clay liner performance characteristics. In *Geotechnical Special Publication*, number 46 /1, pages 421–433, New Orleans, LA, USA, 1995. ASCE.

R. Khanzode, S. Vanapalli, and D. Fredlund. Measurement of soil-water characteristic curves for fine-grained soils using a small-scale centrifuge. *Canadian Geotechnical Journal*, 39(5):1209–1217, 2002. ISSN 00083674.

J. P. Krohn and J. E. Slosson. Assessment of expansive soils in the united states. In *Fourth Intern. Conf. on Expansive Soils*, 1980.

J. Kuhn. Effect of cracking on the hydraulic properties of unsaturated highly plastic clays. Master's thesis, University of Texas, 2005.

R. Lytton, C. Aubeny, and R. Bulut. Design procedure for pavements on expansive soils: Volume 1. Technical Report 0-4518-1, Texas Transportation Institute, 2006.

J. S. McCartney. *Determination of the Hydraulic Characteristic of Unsaturated Soils Using a Centrifuge Permeameter*. PhD thesis, University of Texas, 2007.

A. K. Mishra, S. Dhawan, and S. M. Rao. Analysis of swelling and shrinkage behavior of compacted clays. *Geotechnical and Geological Engineering*, 26(3):289–298, 2008. ISSN 09603182.

N. V. Nayak and R. W. Christensen. Swelling characteristics of compacted expansive soils. *Clays and Clay Minerals*, 19 (4):251–261, 1974.

J. R. Nimmo and K. A. Mello. Centrifugal techniques for measuring saturated hydraulic conductivity. *Water Resources Research*, 27 (6):1263–1269, 1991.

J. R. Nimmo, J. Rubin, and D. P. Hammermeister. Unsaturated flow in a centrifugal field' measurement of hydraulic conductivity and testing of darcy's law. *Water Resources Research*, 23:124–134, 1987.

R. E. Olson. Expansive clay course notes. None, 2009.

M. O'Neill and N. Poormoayed. Methodology for foundations on expansive clays. *Journal of Geotechnical Engineering*, Vol. 106, No. 12:1345–1367, 1980.

A. Rao, B. Phanikumar, and S. R.S. Prediction of swelling characteristics of remoulded and compacted expansive soils using free swell index. *Quarterly Journal of Engineering Geology and Hydrogeology*, 37:217–226, 2004.

A. M. G. Robertson and F. M. Wagener. Lateral swelling pressures in active clay. *1*, 1:107–114, 1975.

C. Savvidoil, P. Culligan, C. Savvidoii, and P. Ctilligan. The application of centrifuge modelling to geo-environmental problems. *Proceedings of the Institution of Civil Engineers: Geotechnical Engineering*, 131(3):152–162, 1998. ISSN 13532618.

H. Seed, R. Woodward, and R. Lundgren. Prediction of swelling potential for compacted clays. *Jornal of the Soil Mechanics & Foundation Engineering Division, American Society of Civil Engineers*, 88 (3):53–87, 1962.

J. S. Sharma and L. Samarasekera. Effect of centrifuge radius on hydraulic conductivity measured in a falling-head test. *Canadian Geotechnical Journal*, 44:96–102, 2007.

J. Simunek and J. R. Nimmo. Estimating soil hydraulic parameters from transient flow experiments in a centrifuge using parameter optimization technique. *Water Resources Research*, 41:1, 2005.

D. Singh and S. J. Kuriyan. Estimation of hydraulic conductivity of unsaturated soils using a geotechnical centrifuge. *Canadian Geotechnical Journal*, 39:684–694, 2002.

D. N. Singh and A. K. Gupta. Modelling hydraulic conductivity in a small centrifuge. *Canadian Geotechnical Journal*, 37:1150–1155, 2000.

D. R. Snethen. Evaluation of expedient methods for identification and classification of potentially expansive soils. In *Proc., Fifth Intern. Conf. on Expansive Soils*, pages 22–26, 1984.

C. Tan and R. Scott. Centrifuge scaling considerations for fluid-particle systems. *Geotechnique*, Vol. 35, No. 4:461–470, 1985.

R. Taylor. Discussion on tan & scoot (1985). *Geotechnique*, Vol. 37, No. 1:131–133, 1985.

TEX-124-E. Determining potential vertical rise. *Texas Department of Transportation*.

N. Thusyanthan and S. Madabhushi. Scaling of seepage flow velocity in centrifuge models. Cambridge University Notes, March 2003.

V. Vijayavergiya and O. Ghazzaly. Prediction of swelling potential for natural clays. In *Proceedings of the 3rd International Conference on Expansive Soils, Haifa, Israel*, volume 1, pages 227–236, 1973.

E. Weisberg and S. Frydman. Study of flow in compacted columns of swelling clay. 1990.

Y. Xie, Z.-H. Chen, S.-G. Sun, G. Li, and X.-W. Fang. Test research on three-dimensional swelling pressure of remolded expansive clay. *Yantu Lixue/Rock and Soil Mechanics*, 28(8):1636–1642, 2007. ISSN 10007598.

A. Zelikson. Hydro-geotechnical modelling on large centrifuges. In *Proceedings of a Symposium on the Application of Centrifuge Modelling to Geotechnical Design.*, pages 155–170, Manchester, Engl, 1985. A. A. Balkema.

Vita

Michael David Plaisted was born in Urbana, Illinois on April 30, 1984, to his parents Anne and David Plaisted. He attended Cresset Christian Academy in Durham, NC. In 2002, he enrolled at North Carolina State University and in December, 2006, graduated Valedictorian with a Bachelors of Science in Civil Engineering. In August, 2007, he began graduate school at the University of Texas at Austin.

Permanent Address: 5616 Hideaway Dr.
Chapel Hill, NC 27516

This thesis was typeset by the author.